

1 Impacts of Tibetan Plateau uplift on atmospheric 2 dynamics and associated precipitation $\delta^{18}\text{O}$

3

4 S. Botsyun¹, P. Sepulchre¹, C. Risi², and Y. Donnadieu¹

5 [1]{Laboratoire des Sciences du Climat et de l'Environnement, LSCE/IPSL, CEA-
6 CNRS-UVSQ, Université Paris-Saclay, Gif-sur-Yvette, France}

7 [2]{Laboratoire de Météorologie Dynamique, LMD/IPSL, UPMC, CNRS, Paris, France}

8 Correspondence to: S. Botsyun (svetlana.botsyun@lsce.ipsl.fr)

9

10 Abstract

11 Paleoelevation reconstructions of mountain belts have become a focus of modern science
12 since surface elevation provides crucial information for understanding both geodynamic
13 mechanisms of Earth's interior and influence of mountains growth on climate. Stable
14 oxygen isotopes paleoaltimetry is one of the most popular techniques nowadays, and
15 relies on the difference between $\delta^{18}\text{O}$ of paleo-precipitation reconstructed using the
16 natural archives, and modern measured values for the point of interest. Our goal is to
17 understand where and how complex climatic changes linked with the growth of
18 mountains affect $\delta^{18}\text{O}$ in precipitation. For this purpose, we develop a theoretical
19 expression for the precipitation composition **based on the Rayleigh distillation and** the
20 isotope-equipped atmospheric general circulation model LMDZ-iso **outputs**. Experiments
21 with reduced height over the Tibetan Plateau and the Himalayas have been designed. Our
22 results show that the isotopic composition of precipitation is very sensitive to climate
23 changes related with the growth of the Himalayas and Tibetan Plateau. **Specifically our**
24 **simulations suggest that only 40% of sampled sites for paleoaltimetry depict a full**
25 **topographic signal, and that uplift-related changes in relative humidity (northern region)**
26 **and precipitation amount (southern region) could explain absolute deviations of up to**
27 **2.5% of the isotopic signal, thereby creating biases in paleoelevation reconstructions.**

28

29

1 1 Introduction

2 Despite ongoing debates regarding the thermal and mechanical nature of mechanisms
3 involved (Boos, 2015; Chen et al., 2014), the Himalayas and the Tibetan Plateau
4 (hereafter TP) have long been considered to exert major influences on Asian atmospheric
5 dynamics, notably by reinforcing South Asian monsoon and driving subsidence
6 ultimately leading to onsets of deserts over Central Asia (Rodwell and Hoskins, 2001;
7 Broccoli and Manabe, 1992). Thus, reconstructing the history of Himalayas and TP uplift
8 appears crucial to understand long-term climate evolution of Asia. On the other hand,
9 ~~topography uplift of TP is ultimately driven by collision between India and Asia~~
10 ~~continents (Molnar et al., 2010), making~~ the timing and scale of surface elevation growth
11 ~~are~~ widely used for reconstructing the rate and style of this tectonic plates convergence
12 (eg. Royden et al., 2008; Tapponnier et al., 2001).

13 Elevation reconstructions for the Tibetan Plateau and Himalayas are based on fossil-leaf
14 morphology (eg. Antal, 1993; Forest et al., 1999; Khan et al., 2014; (Sun et al., 2015),
15 pollen (Dupont-Nivet et al., 2008), correlation between stomatal density and the decrease
16 in CO₂ partial pressure with altitude (McElwain, 2004), and carbonate oxygen isotopic
17 compositions (Currie et al., 2005; DeCelles et al., 2007; Garzzone et al., 2000a; Li et al.,
18 2015; Rowley and Currie, 2006; Saylor et al., 2009; Xu et al., 2013). In contrast to
19 paleobotanical methods, oxygen isotope paleoaltimetry has been widely applied to the
20 Cenozoic. Carbonate $\delta^{18}\text{O}$ is related to topography change using $\delta^{18}\text{O}$ -elevation
21 relationship. These relationships have been calibrated both empirically (Garzzone et al.,
22 2000b; Gonfiantini et al., 2001; Poage and Chamberlain, 2001) and theoretically, using
23 basic thermodynamic principles, including Rayleigh distillation, that govern isotopic
24 fractionation processes (Rowley and Garzzone, 2007; Rowley et al., 2001).

25 The difference between paleoprecipitation $\delta^{18}\text{O}$ detected from natural archives and
26 modern values of the site of interest is identified with the effect of the surface uplift in
27 numerous recent studies (Currie et al., 2005; Cyr et al., 2005; Ding et al., 2014; Hoke et
28 al., 2014; Mulch, 2016; Rowley and Currie, 2006; Rowley et al., 2001; Xu et al., 2013).
29 In the absence of direct measurements of “paleo” altitude- $\delta^{18}\text{O}$ relationship *in situ*, stable-
30 isotope paleoaltimetry is potentially hampered by the fact that the presumed constancy of
31 altitude- $\delta^{18}\text{O}$ relationships through time might not be valid. For instance for the Andes,
32 not considering the impact of uplift on climate dynamics and related $\delta^{18}\text{O}$ values has been

1 shown to produce errors in paleoelevation reconstruction reaching up to $\pm 50\%$ (Ehlers
2 and Poulsen, 2009; Poulsen et al., 2010). Regional climate variables and associated
3 isotopic signal in precipitation can also be affected by global climate change (Battisti et
4 al., 2014; Jeffery et al., 2012; Poulsen and Jeffery, 2011). Moreover, it has been
5 suggested that climate-driven changes in surface ocean $\delta^{18}\text{O}$ through the Cenozoic can
6 also influence recorded values of precipitation $\delta^{18}\text{O}$ over the continent and corrections
7 has been applied in some studies (Ding et al., 2014). Over TP, mismatches between
8 paleoelevation estimations from palynological and stable isotope data (eg. Sun et al.,
9 2014) could be related to complex climatic changes and associated variations of altitude-
10 $\delta^{18}\text{O}$ relationship linked to the uplift, but still a detailed assessment of the consequences
11 of topographic changes on precipitation $\delta^{18}\text{O}$ is lacking.

12 Spatial distribution of isotopes in precipitation was described using various types of
13 models, from one-dimensional to three-dimensional general circulation (Craig, 1961;
14 Dansgaard, 1964; Gedzelman and Arnold, 1994; Risi et al., 2010; Stowhas and Moyano,
15 1993). Such modelling studies show how large-scale Asian monsoon circulation
16 influence precipitation $\delta^{18}\text{O}$ (He et al., 2015; LeGrande and Schmidt, 2009; Pausata et al.,
17 2011; Vuille et al., 2005). At the global scale, precipitation $\delta^{18}\text{O}$ has been shown to be
18 affected by several factors other than elevation, including mixing between air masses
19 (Ehlers and Poulsen, 2009; Gat, 1996), large-scale subsidence (e.g. Frankenberg et al.,
20 2009), continental recycling (Lee et al., 2012; Risi et al., 2013), deep convection (Risi et
21 al., 2008), and enrichments linked to global warming (Poulsen and Jeffery, 2011).
22 Numerous studies have investigated the impact of Asian topography on climate change,
23 including the monsoon intensification (ex. An et al., 2015; Harris, 2006a; Kutzbach et al.,
24 1989; Ramstein et al., 1997; Raymo and Ruddiman, 1992; Zhang et al., 2015) and Asian
25 interior aridification onset (Broccoli and Manabe, 1992; Liu et al., 2015). Nonetheless the
26 linkage between these “climatic parameters” altered by the growth of TP and their
27 influence on the isotopic signal remain unclear. In this article we use numerical
28 modelling to provide some insights.

29

1 **2 Methods**

2 **2.1 Model simulations**

3 We use an Atmospheric General Circulation model (GCM) developed at Laboratoire de
4 Météorologie Dynamique, Paris, France with isotopes-tracking implement, called LMDZ-
5 iso (Risi et al., 2010). LMDZ-iso is derived from the LMDz model (Hourdin et al., 2006)
6 that has been used for numerous future and paleoclimate studies (Ladant et al., 2014;
7 Pohl et al., 2014; Sepulchre et al., 2006). Water in a condensed form and its vapour are
8 advected by the Van Leer advection scheme (Van Leer, 1977). Isotopic processes in
9 LMDZ-iso are documented in (Risi et al., 2010). Evaporation over land is assumed not to
10 fractionate, given the simplicity of the model surface parameterisation (Risi et al., 2010).
11 Yao et al. (2013) have provided a precise description of rainfall patterns over the TP, and
12 showed LMDZ-iso ability to simulate atmospheric dynamics and reproduce rainfall and
13 $\delta^{18}\text{O}$ patterns consistent with data over this region.

14 LMDZ-iso is also equipped with water tagging capabilities, allowing us to quantify
15 different moisture contributions from continental and oceanic evaporation sources. The
16 advantage of this technique compared to typical back-trajectories methods is that it tracks
17 the water rather than air masses, thus taking into account effects of phase changes. In our
18 simulations five potential moisture sources are considered: (1) continental sources, (2)
19 Indian Ocean, (3) Atlantic Ocean, (4) Mediterranean Sea, and (5) Pacific Ocean.

20 We use a model configuration with 96 grid points in longitude, 72 in latitude and 19
21 vertical layers, with the first four layers in the first kilometer above the surface. LMDZ-
22 iso has a stretchable grid that allows increased spatial resolution over a defined region. In
23 our case, it gives an averaged resolution of ~ 100 km over central Asia, which is a good
24 trade-off between a reasonable computing time and a spatial resolution that adequately
25 represents main features of TP topography.

26 Here we report results from three experiments designed to isolate the influence of Asian
27 topography on climate and isotopic composition of precipitation. Topography is derived
28 from a 10-minute US Navy dataset and interpolated to the model grid. The control run
29 (MOD) is a pre-industrial run, i.e. initialized with boundary conditions (insolation,
30 greenhouse gases, sea surface temperatures (SSTs), topography) kept at pre-industrial
31 values. For the two other experiments, we keep all boundary conditions (including
32 albedo, rugosity, and vegetation distribution) similar to those in MOD run, except for the

1 topography. We reduce the altitude over the area covering the Tibetan Plateau, Himalayas
2 and a part of surrounding mountains: Tian Shan, Pamir, Kunlun and Hindu Kush to 50%
3 of modern elevations (intermediate, INT case) and to 250-m elevation (low, LOW case)
4 (Fig. 1). SSTs for all runs come from the AMIP dataset (monthly SSTs averaged from
5 1979 to 1996; Taylor et al., 2000). Each experiment has been run for 20 years. We
6 analyse seasonal means over the last 18 years, as the two first years are extracted for spin-
7 up.

8 **2.2 Theoretical framework for the precipitation composition**

9 Our goal is to understand to what extent topography changes explain the precipitation
10 $\delta^{18}\text{O}$ signal over TP (i.e. the direct topography effect) and what part of this signal
11 depends on other climate processes. To do so, we develop a theoretical expression for the
12 precipitation composition.

13 To the first order, the $\delta^{18}\text{O}$ composition of the precipitation R_p follows that of the vapour
14 R_v . Deviations from the vapour composition, $\varepsilon = R_p - R_v$, are associated with local
15 condensational or post condensational process.

$$16 \quad R_p = R_v + \varepsilon \quad (1)$$

17 In an idealized framework of an isolated air parcel transported from an initial site at low
18 altitude to the site of interest (Fig. 2), the vapour composition can be predicted by
19 Rayleigh distillation:

$$20 \quad R_v = R_{v0} \cdot f^{\alpha-1} + \delta R_v \quad (2)$$

21 where R_{v0} is the initial composition of the vapour at the initial site, α is the fractionation
22 coefficient, that depends on temperature and on the water phase (Majzoube, 1971;
23 Merlivat and Nief, 1967), and f is the residual fraction of the vapour at the site of interest
24 relatively to the initial site. We take the initial site as characterised by a temperature and
25 humidity T_0 and q_0 . Under these conditions, R_{v0} is the theoretical isotopic composition of
26 vapour that it would have if all the vapour originated from the local evaporation over
27 quiescent oceanic conditions. Depending on the atmospheric circulation, on deep
28 convective and mixing processes and on the source region of water vapour, the isotopic
29 composition of vapour may deviates from the Rayleigh distillation by δR_v .

30 The residual fraction f depends on the specific humidity q at the site of interest:

1 $f = q/q_0$ (3)

2 The air is not always saturated near the surface:

3 ~~where q_s is the saturation specific humidity, function of temperature following the~~
 4 ~~Clausius-Clapeyron relationship.~~

5 ~~If we assume that the air at the site of interest has been transported adiabatically from the~~
 6 ~~area of minimum condensation temperature, then:~~

7 $q = h \cdot q_s(T_s)$ (4)

8 where h and T_s are the relative humidity and air temperature near the surface of the site of
 9 interest. The air can be under-saturated because it can be considered as air that has been
 10 transported adiabatically from the area of minimum condensation temperature, T^*
 11 (Galewsky and Hurley, 2010; Galewsky et al., 2005; Sherwood, 1996): $q=q_s(T^*)$

12 The surface temperature can be predicted to first order by the adiabatic lapse rate, Γ , and
 13 is modulated by the non-adiabatic component δT_s that represents processes such as large-
 14 scale circulation or radiation:

15 $T_s = T_0 + \Gamma \cdot (z - z_0) + \delta T_s$ (5)

16 where z and z_0 are the altitudes at the site of interest and at the initial site. We use an
 17 adiabatic lapse rate equal to 5° km^{-1} based on the measurements of modern observed
 18 mean temperature lapse rate on the southern slope of the central Himalayas, that ranges
 19 from 4.7 to $6.1^\circ \text{ km}^{-1}$ for the monsoon season and from 4.3 to $5.5^\circ \text{ km}^{-1}$ for the rest of the
 20 year (Kattel et al., 2015).

21 If we combine Eq. (1) to Eq. (5), we get that R_v is a function of ε , δR_v , h , δT_s and z :

22 $R_p = R_{v0} \cdot [h \cdot q_s(T_0 + \Gamma \cdot (z - z_0) + \delta T_s)/q_0]^{\alpha-1} + \delta R_v + \varepsilon$ (6a)

23 Or in a simpler form:

24 $R_p = R_p(\varepsilon, \delta R_v, h, \delta T_s, z)$ (6b)

25 Parameters z_0 , q_0 , T_0 are reference values that are common to all sites of interest, all
 26 climates and geographies. Even if initial conditions for the Rayleigh distillation vary
 27 depending on the atmosphere circulation, on deep convective processes and on the site of
 28 interest, we keep the same reference values and we consider all variations in initial
 29 conditions are accommodated by δR_v .

1 This model is equivalent to that of Rowley et al. (2001) for $\delta R_v = 0$ (i.e. neglecting the
 2 effects of mixing and deep convection on the initial water vapour), $\varepsilon = (\alpha - 1) \cdot R_v$ (i.e.
 3 neglecting post-condensational effects), and $h = 1$ (i.e. assuming the site of interest is
 4 inside the precipitating cloud).

5 **2.3 Decomposing precipitation composition differences**

6 Our goal is to understand why R_p varies from one climatic state to another. We refer to
 7 these climatic states using subscript 1 and 2 and to their difference using the Δ notation.
 8 Differences between INT and LOW and between MOD and INT climatic states
 9 corresponds to the initial and the terminate stages of the TP uplift respectively. We
 10 decompose $\Delta R_p = R_{p2} - R_{p1}$ into contribution from $\Delta \delta R_v$, $\Delta \varepsilon$, Δh , $\Delta \delta T_s$, and Δz :

$$11 \quad \Delta R_p = \frac{\partial R_p}{\partial \delta R_v} \cdot \Delta \delta R_v + \frac{\partial R_p}{\partial \varepsilon} \cdot \Delta \varepsilon + \frac{\partial R_p}{\partial h} \cdot \Delta h + \frac{\partial R_p}{\partial \delta T_s} \cdot \Delta \delta T_s + \frac{\partial R_p}{\partial z} \cdot \Delta z \quad (8)$$

$$12 \quad \Delta R_p = \Delta R_{p,\Delta \varepsilon} + \Delta R_{p,\Delta \delta R_v} + \Delta R_{p,\Delta h} + \Delta R_{p,\Delta \delta T_s} + \Delta R_{p,\Delta z} + N \quad (7)$$

13 Where $\Delta R_{p,\Delta \varepsilon}$, $\Delta R_{p,\Delta \delta R_v}$, $\Delta R_{p,\Delta h}$, $\Delta R_{p,\Delta \delta T_s}$, and $\Delta R_{p,\Delta z}$ are respectively the contributions of
 14 $\Delta \delta R_v$, $\Delta \varepsilon$, Δh , $\Delta \delta T_s$, and Δz to ΔR_p . Non linear terms of decomposition are gathered into
 15 the residual term N . Contributions are estimated using equation 6 (see also Table 1):

$$16 \quad R_{p,\Delta \varepsilon} = R_p(\varepsilon_2, \delta R_v', h', \delta T_s', z') - R_p(\varepsilon_1, \delta R_v', h', \delta T_s', z') \quad (8)$$

$$17 \quad R_{p,\Delta \delta R_v} = R_p(\varepsilon', \delta R_{v2}, h', \delta T_s', z') - R_p(\varepsilon', \delta R_{v1}, h', \delta T_s', z') \quad (9)$$

$$18 \quad R_{p,\Delta h} = R_p(\varepsilon', \delta R_v', h_2, \delta T_s', z') - R_p(\varepsilon', \delta R_v', h_1, \delta T_s', z') \quad (10)$$

$$19 \quad R_{p,\Delta \delta T_s} = R_p(\varepsilon', \delta R_v', h', \delta T_{s2}, z') - R_p(\varepsilon', \delta R_v', h', \delta T_{s1}, z') \quad (11)$$

$$20 \quad R_{p,\Delta z} = R_p(\varepsilon', \delta R_v', h', \delta T_s', z_2) - R_p(\varepsilon', \delta R_v', h', \delta T_s', z_1) \quad (12)$$

21 In order to decrease the sensitivity of the decomposition to the state at which it has been
 22 calculated we take z' , $\delta T_s'$, h' , $\delta R_v'$, and ε' as centred differences:

$$23 \quad z' = (z_2 + z_1)/2 \quad (13)$$

$$24 \quad \delta T_s' = (\delta T_{s2} + \delta T_{s1})/2 \quad (14)$$

$$25 \quad h' = (h_2 + h_1)/2 \quad (15)$$

$$26 \quad \delta R_v' = (\delta R_{v2} + \delta R_{v1})/2 \quad (16)$$

$$27 \quad \varepsilon' = (\varepsilon_2 + \varepsilon_1)/2 \quad (17)$$

28 Note that ε' in Equations 9 to 12 and $\delta R_v'$ in Equations 8 and 10 to 12 can be replaced by

0 without changing the result. Parameters z , δT_s , h , δR_v , and ε are diagnosed for the climatic states 1 and 2 from LMDZ-iso simulations (ex. for pairs of experiments, MOD and INT cases). Parameter ε is estimated as $\varepsilon = R_p - R_v$, where R_p and R_v are isotopic ratios simulated by LMDZ-iso. Parameter h is the relative humidity simulated by LMDZ-iso. Altitude z is a prescribed boundary condition of the simulations. Parameter δR_v is estimated by calculating the difference between the water vapour isotopic ratio simulated by LMDZ-iso ($R_{v,LMDZ}$) and that predicted by Rayleigh distillation if the initial water vapour isotopic ratio is R_{v0} :

$$\delta R_v = R_{v,LMDZ} - R_{v0} \cdot (q/q_0)^{\alpha-1} \quad (18)$$

where q is the specific humidity simulated by LMDZ-iso and α is the isotopic fractionation as a function of the near-surface air temperature T_s simulated by LMDZ-iso. Parameter δT_s is estimated from equation (5) by calculating the difference between the near-surface air temperature simulated by LMDZ-iso and that predicted by the adiabatic lapse rate:

$$\delta T_s = T_s - T_0 - \Gamma \cdot (z - z_0) \quad (19)$$

~~To estimate each of these terms, we estimate difference between R_p calculated from the different values of δR_v , ε , h , δT_s , and z , changing only one parameter at a time, as detailed in table 1 (and see next section).~~

~~Values of δR_v , ε , h , δT_s , and z , are diagnosed using LMDZ-iso simulations. As an example $R_p(\delta R_{v1}, \varepsilon_2, h_2, \delta T_{s2}, z_2)$ is the precipitation composition simulated by LMDZ for climate state 2. As another example, $R_p(0,0,1, \delta T_{s1}, z_1)$ is the precipitation composition predicted by Eqs. (2)-(5) with $\delta R_{v1} = 0$ and using the near-surface air temperature as T_s simulated by LMDZ for climatic state 1 (see Table 1).~~

All the isotopic decomposition terms computed are weighted by the precipitation amount.

2.4 Robustness of the decomposition

First, to check whether the linear decomposition is a good approximation of the total R_p change, we estimate the non-linear term N as a residual, i.e. for each pair of states, we calculate the deviation of $\Delta R_p = R_p(\varepsilon_2, \delta R_{v2}, h_2, \delta T_{s2}, z_2) - R_p(\varepsilon_1, \delta R_{v1}, h_1, \delta T_{s1}, z_1)$ from LMDZ-simulated isotopic differences between the two experiments. N represents less than 17% of the total R_p change for both stages of TP uplift.

1 Our method to estimate the terms in Eq. (7) is equivalent to first order approximation of
2 partial derivatives, i.e. we neglect the sensitivity of the partial derivatives to the state at
3 which they are calculated. We tested this sensitivity by using Eq. (8) to Eq. (12) changing
4 z' to z_1 or z_2 $\delta T_s'$ to δT_{s2} or δT_{s1} and so on. For example, in Eq. (12), replacing of h' by
5 h_1 changes the resulting $R_{p,\Delta z}$ by 0.03‰, replacing of h' by h_2 has an impact of 0.09‰. In
6 the same equation, replacing of $\delta T_s'$ by δT_{s1} and by δT_{s2} contributes to $R_{p,\Delta z}$ by 0.005‰
7 and 0.039‰ respectively. As it was highlighted earlier, replacing of ε' and $\delta T_s'$ by ε_1 or ε_2
8 and δR_{v1} or δR_{v2} respectively has no impact to the resulting $R_{p,\Delta z}$. Thus our method show
9 low sensitivity to the state.

10 Second, to check the influence of initial conditions R_{v0} , T_0 and q_0 on the
11 decomposition, we estimate the sensitivity of the different contributions to changes in
12 R_{v0} , T_0 , and q_0 , of 1%, 1K and 10% respectively (Table 2). R_{v0} is the parameter that
13 influences the most the decomposition terms, with a maximal sensitivity obtained of
14 0.9‰ for $\Delta R_{p,\Delta z}$ for a change of 1‰ in R_{v0} . Sensitivity to temperature and humidity are
15 lower, ranging from 0 to 0.6‰. Overall, all the decomposition terms show a sensitivity
16 <1‰ with most (82%) of them <0.5‰, making our decomposition method robust.

17

18 **3 Results**

19 **3.1 Model validation in terms of simulated climate variables**

20 LMDZ has been used for numerous present-day climate and paleoclimate studies
21 (Kageyama et al., 2005; Ladant et al., 2014; Sepulchre et al., 2006), including studies of
22 monsoon region (eg. Lee et al., 2012; Licht et al., 2014). Yao et al., (2013) showed that
23 LMDZ-iso has the best representation of the altitudinal effect compared to similar GCM
24 and RCM models. These authors also have provided a detailed description of rainfall
25 patterns over the Tibetan Plateau, and showed LMDZ-iso ability to simulate atmospheric
26 dynamics and reproduce rainfall and $\delta^{18}\text{O}$ patterns consistent with data over this region.
27 For the purpose of our experiments validation, we compare MOD experiment outputs
28 with rainfall data from the Climate Research Unit (CRU) (New et al., 2002) (Fig. 3 A B
29 C). When compared to CRU dataset, MOD annual rainfalls depict an overestimation over
30 the high topography of the Himalayas and the southern edge of the Plateau, with a rainy
31 season that starts too early and ends too late in the year. Over central Tibet (30-35°N), the

1 seasonal cycle is well captured by LMDz-iso, although monthly rainfall is always slightly
2 overestimated (+0.5 mm/day). CRU data shows that the northern TP (35-40°N) is dryer
3 with no marked rainfall season and a mean rainfall rate of 0.5 mm/day. In MOD
4 experiment, this rate is overestimated (1.5 mm/day on annual average). Despite these
5 model-data mismatches, the ability of LMDZ-iso to represent the seasonal cycle in the
6 south and the rainfall latitudinal gradient over the TP allows its use for the purpose of this
7 study.

8 Our MOD simulation is pre-industrial, consequently a comparison with modern data is
9 expected to provide differences driven by the pre-industrial boundary conditions. Still
10 comparing LMDZ-iso outputs with mean annual temperatures from CRU dataset (New et
11 al., 2002) (Fig. 3 D E F) and relative humidity from NCEP-DOE Reanalysis (Kanamitsu
12 et al., 2002) (Fig. S1) shows that LMDZ-iso model captures these variables reasonably
13 well.

15 3.2 Impact of TP uplift on Asian climate

16 Theoretically, the Tibetan Plateau has both mechanical and thermal effects on
17 atmospheric dynamics that induce increase monsoon activity to the south and drive arid
18 climate to the north (Broccoli and Manabe, 1992; Sato and Kimura, 2005). Thus
19 modifying TP height is expected to alter these large-scale atmospheric dynamics and
20 associated climate variables (namely temperature, precipitation, relative humidity
21 (hereafter RH), cloud cover), and in turn to affect the isotopic signature of rainfall.

22 In LOW experiment, strong summer heating leads to the onset of a “Thermal Low” (TL)
23 at the latitude of maximal insolation (ca. 32°N), similar to the present-day structure TL
24 existing over the Sahara desert (Fig. S2). This structure is superimposed by large-scale
25 subsidence linked to the descending branch of the Hadley cell, and both factors act to
26 drive widespread aridity over TP area between ca. 30°N and 40°N, associated with very
27 low (<40%) RH values (Fig. S2). Subsidence also prevents the development of South
28 Asian monsoon over the north Indian plane and favours aridity over this region. In
29 winter, large-scale subsidence induces high surface pressures and creates an anticyclonic
30 cell that prevents convection and humidity advection, resulting in low RH and annual
31 rainfall amount ranging from 50 to 500 mm over TP area (Fig. 4).

1 Uplifting TP from 250m above sea-level (ASL) to half of its present-day altitude (INT
2 case) initiates convection in the first tropospheric layers, **restricting** large-scale
3 subsidence to the upper levels (Fig. 4). In turn, south Asian monsoon is strengthened and
4 associated northward moisture transport and precipitation increase south of TP (Fig. 5, 6).
5 As a consequence the hydrological cycle over TP is more active, with higher evaporation
6 rates (Fig. 7 D). Together with colder temperatures linked to higher altitude (adiabatic
7 effect) (Fig. 7 B), the stronger hydrological cycle drives an increase in RH (Fig. 7 A) and
8 cloud cover (Fig. S3). Another consequence of increased altitude is higher snowfall rates
9 in winter and associated rise of surface albedo (fig. S4). When added to the increased
10 cloud cover effect, this last process contributes to an extra cooling of air masses over the
11 Plateau. To the north of TP, the initial stage of uplift results in increased aridity (i.e.
12 lower RH and rainfall) over the Tarim Basin region. This pattern can be explained both
13 by a barrier effect of southern topography and by stationary waves strengthening, that
14 results in subsidence to the north of TP. This latter mechanism is consistent with pioneer
15 studies which showed that mountain-related activation of stationary waves prevented
16 cyclonic activity over Central Asia and induced aridity over this region (Broccoli and
17 Manabe, 1992).

18 The impact of the terminal stage of TP uplift also drives an increase in RH over the
19 Plateau, especially during summer time, when a very active continental recycling (Fig.
20 S6) makes RH rise from 40% (INT) to 70% (MOD). Precipitation amount also increases
21 significantly (Fig. 6), driven both by increased evaporation and water recycling during
22 summer, and intense snowfall during winter. The latter contributes to increase the surface
23 albedo and associated surface cooling during winter. Conversely, the uplift to a modern-
24 like Plateau reduces RH (down to 30%) north of the Plateau, and allows the onset of large
25 arid areas. We infer that this aridification is linked to a mechanical blocking of moisture
26 transport, both by Tian Shan topography for the winter westerlies, and the eastern flanks
27 of TP for summer fluxes, since despite changes in stationary waves structure and sensible
28 heat (not shown), no marked shift in subsidence between INT and MOD experiments is
29 simulated. This result is consistent with recent studies (Miao et al., 2012; Sun et al.,
30 2009) that have suggested the potential contribution of Pamir and Tian Shan rainshadow
31 effect to aridification in Qaidam Bassin and creation of Taklamakan Desert.

32

1 3.3 Response of precipitation $\delta^{18}\text{O}$ to TP uplift

2 3.3.1 Model validation in terms of simulated precipitation $\delta^{18}\text{O}$

3 The modern mean annual isotopic distribution is characterised by very depleted values of
4 $\delta^{18}\text{O}$ over the Himalayas and the southern Tibet (down to -18‰) and a shift to more
5 positive values (ranges from -11 to -13‰) over northern TP and Kunlun from 30°N to
6 35°N . Precipitation $\delta^{18}\text{O}$ over Tarim Basin experiences an abrupt decrease compared to
7 northern TP, with values down to -16‰ . (Fig. 8 A). Overall, simulated annual mean
8 $\delta^{18}\text{O}_p$ are consistent with sparse observations from the International Atomic Energy
9 Agency (IAEA) Global Network of Isotopes in Precipitation and $\delta^{18}\text{O}$ in precipitation
10 measurements compiled from Quade et al. (2011), Bershaw et al. (2012), Hren et al.
11 (2009), Caves et al. (2015) (Fig. 8 A B). In general, model shows a good agreement with
12 precipitation and VSMOW-weighted modern surface waters $\delta^{18}\text{O}$, including stream, lake
13 and spring waters (data from Bershaw et al., 2012; Hren et al., 2009; Quade et al., 2011),
14 as testified by a Pearson coefficient of 0.86 between modelled and observed precipitation
15 $\delta^{18}\text{O}$ (Fig 8C). This comparison shows the ability of LMDZiso to reproduce the decrease
16 in $\delta^{18}\text{O}$ from India subcontinent to Himalayas foothills and with minimum values over
17 the Himalayas. Simulated increase in $\delta^{18}\text{O}$ over the TP with the distance from the
18 Himalayas is also consistent with data sampled along a southwest-northeast transect
19 across the Plateau (Bershaw et al., 2012). However over the northern margins of the TP,
20 LMDZ-iso underestimates simulated $\delta^{18}\text{O}$ in precipitation. This model-data mismatch
21 may result from two types of uncertainties. First despite the high resolution obtained with
22 a zoomed grid, restricted topographic features could be not well-captured over some parts
23 of the TP, which could lead our simulations to miss local processes affecting $\delta^{18}\text{O}$ in
24 rainfall. Second, overestimating the westerlies fluxes (see the comparison with the ERA
25 moisture transport on Fig. 5 A) could lead to underestimate $\delta^{18}\text{O}$ over the northern part of
26 the TP, through advection of depleted air masses. Nevertheless, despite our model does
27 not capture well the absolute maximal values, the regional latitudinal gradient is correctly
28 represented, and most observed values are within the range of simulated $\delta^{18}\text{O}$ (Fig. 8B).
29 We consider that the ability of LMDZ-iso to represent this gradient makes it reliable to
30 carry out this study, which is focusing on sensitivity experiments with large changes in
31 topography and associated anomalies in $\delta^{18}\text{O}$.

32

1 3.3.2 Simulated isotopic changes and signal decomposition

2 To first order, increasing topography over TP leads to more negative $\delta^{18}\text{O}$ over the region
3 (Fig. 9). In the absence of topography, precipitation $\delta^{18}\text{O}$ follows a zonal pattern and
4 undergoes a weak latitudinal depletion on the way to the continental interior, except from
5 slight deviations over India ~~n-plane~~, central China and the Eastern part of the TP (Fig. 9
6 B). At 40°N , i.e. the northern edge of modern TP, $\delta^{18}\text{O}$ values reaches -9‰ in LOW case,
7 compared to -14‰ in MOD case. For the INT case the latitudinal depletion from south to
8 north is stronger (ca. 0.4‰ per latitudinal degree), with $\delta^{18}\text{O}$ values ranging from -6‰
9 for the lowered Himalayas foothills to -11‰ for northern and eastern margins of TP (Fig.
10 9 A).

11 The total difference in isotopic composition of precipitation, ΔR_p , between pairs of
12 experiments (INT-LOW, MOD-INT) is significant beyond the areas where the
13 topography was reduced by the experimental design (Fig. 10 A, Fig. 11 A). Substantial
14 differences in $\delta^{18}\text{O}$ between MOD and INT experiments are simulated over the southern
15 TP (up to 10‰) and over the Tarim Basin (up to 7‰). Between INT and LOW cases, the
16 differences are over the margins of the TP, over Pamir, Tian Shan and Nan Chan. We
17 should note that the isotopic difference becomes more important for the later stage of the
18 plateau uplift. For clarity, we define two boxes, over the northern (from 34°N to 38°N
19 and from 88°E to 100°E) and southern (from 27°N to 33°N and from 75°E to 95°E) part
20 of TP.

21

22 Direct topography effect on $\delta^{18}\text{O}$

23 The direct effect of topography change is determined as the decomposition term $\Delta R_{p,\Delta z}$
24 $\frac{\partial R_p}{\partial z} \cdot \Delta z$ in Eq. (7). For the initial stage of the uplift, the altitude effect produces a
25 decrease in precipitation $\delta^{18}\text{O}$ ranging from -1 to -3‰ (Fig. 10 B). For the terminal stage
26 of the uplift, the isotopic decrease linked with altitude goes up to -7‰ (Fig. 11 B).
27 Differences between both stages are linked to the non-linear relationship between $\delta^{18}\text{O}$
28 and elevation. Also for both stages, the difference between ΔR_p and $\Delta R_{p,\Delta z} \frac{\partial R_p}{\partial z} \cdot \Delta z$ is
29 non-zero (Fig. 12 A, Fig. 13 A). These differences are particularly marked for the
30 terminal stage, for which $\Delta R_{p,\Delta z} \frac{\partial R_p}{\partial z} \cdot \Delta z$ averages -5.5‰ over the northern part of TP

1 (Fig. 13 A B), whereas the total isotopic change averages -3‰. Locally, the difference
 2 between $\Delta R_{p,\Delta z} \frac{\partial R_p}{\partial z} \cdot \Delta z$ and ΔR_p can reach +4‰. When averaged over the southern box,
 3 $\Delta R_{p,\Delta z} \frac{\partial R_p}{\partial z} \cdot \Delta z$ is less negative (-4‰) than ΔR_p (-4.6‰), with localized maximum
 4 differences reaching -4‰. Offsets between $\Delta R_{p,\Delta z} \frac{\partial R_p}{\partial z} \cdot \Delta z$ and ΔR_p are also detected for
 5 the initial stage of the uplift (Fig. 12 A B), but are lower: they reach +2‰ over central TP
 6 but barely reach 1‰ when averaged over southern and northern boxes. These offsets are
 7 related to additional effects of uplift on $\delta^{18}\text{O}$ that are discussed in the following sections.

8

9 **Non-adiabatic temperature changes impact**

10 Besides the adiabatic temperature effects linked with the TP uplift, non-adiabatic
 11 temperature changes can be identified, in relation with surface albedo and cloud cover
 12 changes depicted in 3.2.1. The term $\Delta R_{p,\Delta\delta T} \frac{\partial R_p}{\partial \delta T_s} \cdot \Delta \delta T_s$ in Eq. (7) (Table 1, line 3) is
 13 associated with these non-adiabatic effects, i.e. spatial variations of the temperature lapse
 14 rate. Figure 10 C and Figure 11 C show the portion of the total isotopic signal that is
 15 linked to this effect. It plays a modest role for the early phase of uplift (+1-2‰ locally),
 16 but is more important for the second stage. It contributes to 2-5‰ of total isotopic
 17 difference, with a positive sign over southeast TP interior, TP northern margins and Asia
 18 interior. Negative anomalies have ~~the same~~ a magnitude of 2-3‰, but are less
 19 widespread, localized over the TP interior (Fig. 11 C). Positive isotopic anomalies are
 20 associated with steeper lapse rate than expected based on adiabatic processes.
 21 Conversely, negative $\delta^{18}\text{O}$ anomalies that are observed over northern TP and over Pamir
 22 are explained by a weaker lapse rate than adiabatic. Overall, these variations represent
 23 between 10 and 19% (4-10% for the initial stage) of the processes that are not linked to
 24 topography (Fig. 12 D, E and 13 D, E).

25

26 **Impact of RH changes during condensation process**

27 The term $\Delta R_{p,\Delta h} \frac{\partial R_p}{\partial h} \cdot \Delta h$ in Eq. (7) depicts the portion of total isotopic signal ΔR_p linked
 28 to local RH change during condensation process (Table. 1, line 4). Over TP, $\Delta R_{p,\Delta h}$
 29 $\frac{\partial R_p}{\partial h} \cdot \Delta h$ is positive for both uplift phases, and RH changes act as a counterbalance to the

1 topography effect. $\Delta R_{p,\Delta h} \frac{\partial R_p}{\partial h} \cdot \Delta h$ reaches +4‰ for the late stage (Fig. 11 D), and
 2 maxima are located over western part and northern part of TP for both stages of the uplift.
 3 Equation (4) shows that this positive anomaly is directly related to the increase in RH
 4 described in 3.2.1. For the initial stage, $\Delta R_{p,\Delta h} \frac{\partial R_p}{\partial h} \cdot \Delta h$ depicts also positive values (up to
 5 +3‰) to the southwest of TP. When averaged over northern and southern boxes, the
 6 counterbalancing effect of RH on ΔR_p ranges from 1.5 to +3‰, and this effect represents
 7 up to 76% of all non-topographic processes (Fig. 12, 13). Interestingly, an opposite signal
 8 is simulated over the Tarim basin, where topography was kept constant in the three
 9 experiments. This signal is consistent with the previously-depicted decrease in RH over
 10 this region, in relation with rain-shadow effects and large-scale subsidence.

11

12 **Post-condensation processes impact**

13 The difference between $\delta^{18}\text{O}_v$ and $\delta^{18}\text{O}_p$ is linked to the post-condensation effects, mainly
 14 associated with raindrop reevaporation that can occur after initial condensation. Because
 15 lighter isotopes evaporate more easily, rain reevaporation leads to an isotopic enrichment
 16 of precipitation. Therefore, the more reevaporation, the greater the difference between
 17 $\delta^{18}\text{O}_p$ and $\delta^{18}\text{O}_v$. We refer to the study of (Lee and Fung, 2008), where post-condensation
 18 effects are explained in details. The contribution of such processes increases dramatically
 19 for very dry areas, where the relative humidity is less than 40%. Estimation of term $\Delta R_{p,\Delta \epsilon}$
 20 $\frac{\partial R_p}{\partial \epsilon} \cdot \Delta \epsilon$, i.e. the change in isotopic difference between vapour and precipitation, allows to
 21 quantify the contribution of post-condensational processes to total ΔR_p signal (Fig. 10 E,
 22 11 E) without appealing to the d-excess. For both stages of uplift, $\Delta R_{p,\Delta \epsilon} \frac{\partial R_p}{\partial \epsilon} \cdot \Delta \epsilon$ is
 23 mostly negative, indicating a depletion of R_p relatively to R_v with the uplift. Over the
 24 Plateau, contribution of post-condensational effects for the initial stage of uplift ranges
 25 from 25% to 46% of total non-topographic effects, whereas it represents less than 10%
 26 for the terminal stage (Fig. 12 A, 13 A). The most significant signal is simulated over the
 27 northern part of the Plateau and over its western margin and adjacent areas. Post-
 28 condensational effects during the initial stage lead to up to a -5‰ anomaly over the
 29 western margin of TP (Fig. 12 E) whereas the terminal stage creates a substantial
 30 negative anomaly only over northern TP margin and Tarim Basin (Fig. 13 E).

1
2
3
4
5
6
7
8
9
10
11
12
13
14
15
16
17
18
19
20
21
22
23
24
25
26
27
28
29
30
31

Residual processes effect

The last term of Eq. (7), $\Delta R_p \cdot \frac{\partial R_p}{\partial \delta R_p} \cdot \frac{\Delta \delta R_p}{\Delta R_p}$, corresponds to the part of the total isotopic signal that could not be explained by previously mentioned processes. These residual anomalies are rather weak for the initial stage of the uplift, explaining less than 1‰ of the signal over the northern plateau, and around 1‰ over the southern TP and adjacent parts of Asia and India (Fig. 10 F). Contribution of these effects to the initial stage is 4% and 21% to the northern and southern box respectively (Fig. 12 D E). Conversely, for the terminal stage of the TP uplift this anomaly reaches up to -4‰ over the southern part of the TP (Fig. 11 F) and contributes to 49% of the non-topographic processes signal (Fig. 13 D E). In the next sections we propose several mechanisms that could contribute to this residual anomaly.

4 Discussion

Our results suggest that TP uplift affects precipitation $\delta^{18}\text{O}$ through direct topographic effect, but that a significant part of the signal is related to several other processes. These processes alter the isotopic signal not only over TP, but also over adjacent regions, where topography was kept the same by the experiment design. A second result is that despite a similar altitudinal change of TP between the two uplift stages, the topographic effect on $\delta^{18}\text{O}$ is more perturbed by other processes during the terminal stage than during the initial one.

For the terminal stage, the residual effects change over the southern region dominates (49%) the isotopic signal that is not linked to the direct topographic effect. The RH change and non-adiabatic temperature changes also have an important counterbalancing impact, together contributing to 43% of the isotopic signal (Fig. 13 E). For the northern region, the topographic effect is mainly counterbalanced by the RH change effect (2.5‰), ultimately leading to a 2.3‰ offset between ΔR_p and what expected from topography. Here RH contributes to 76% of the isotopic signal not linked with the topography change, while non-adiabatic temperature changes, residual effects change and post-condensational processes have an impact of 16%, 7% and <1% respectively (Fig. 13 D).

1 4.1 Impact of RH variations

2 RH alters rainfall isotopic signature through two steps, during and after condensation. As
3 mentioned earlier, the first effect of RH, as shown in Eq. (4) and expressed as $\Delta R_{p,\Delta h}$
4 $\frac{\partial R_p}{\partial h} \cdot \Delta h$, occurs during condensation through Rayleigh distillation and induces that R_p
5 increases with increasing RH. Our model shows that RH increases over TP with the
6 initial stage of uplift, driving precipitation $\delta^{18}\text{O}$ towards less negative values. This
7 mechanism is more efficient for the terminal stage of uplift, when RH is increased in
8 summer as a response of a more active water cycle. South of TP, RH direct effect on $\delta^{18}\text{O}$
9 is noticeable, as efficient moisture transport is activated with the uplift-driven
10 strengthening of monsoon circulation (Fig. 4). Interestingly, this mechanism is not active
11 for the second stage of the uplift, during which rainfall increases through more effective
12 convection, not through higher advection of moisture. As a consequence, negligible RH
13 and R_p changes are simulated south of the Plateau when it reaches its full height. This
14 suggests that an altitudinal threshold might trigger south Asian monsoon strengthening,
15 and ultimately precipitation $\delta^{18}\text{O}$ signature, a hypothesis that should be explored in
16 further studies. Conversely, the negative values of $\Delta R_{p,\Delta h} \frac{\partial R_p}{\partial h} \cdot \Delta h$ over and northeast of
17 the Tarim basin are related to a decrease in RH during both stages. Our analysis suggests
18 that the first uplift stage is sufficient to create both barrier effects to moisture fluxes and
19 large-scale subsidence that ultimately drive aridity over the region.

20 The second effect of RH on $\delta^{18}\text{O}$ concerns very dry areas (ca. < 40%), where raindrop re-
21 evaporation can occur after initial condensation, leading to an isotopic enrichment of
22 precipitation compared to water vapour (Lee and Fung, 2008) (Fig. S2). Such an effect is
23 implicitly included in the post-condensational term of our decomposition that shows
24 opposite sign when compared to $\Delta R_{p,\Delta h} \frac{\partial R_p}{\partial h} \cdot \Delta h$. Over the Plateau, this mechanism is
25 effective only for the first uplift stage, where TP area transits from very low precipitation
26 amounts and very low RH values to wetter conditions (Fig. S7).

27 Over TP, the opposed effects of RH almost compensate each other for the early stage of
28 the uplift (Fig. 10 D, E), but it is not the case for the final stage, since RH post-
29 condensational effect is similar between INT and MOD experiments. Since absolute
30 values of the impact of RH through condensation and post-condensational processes can

1 reach 5‰, it is crucial to consider RH variation when inferring paleoaltitudes from
2 carbonates $\delta^{18}\text{O}$.

3

4 **4.2 “Amount effect” and monsoon intensification**

5 Our results also show a substantial increase in precipitation amount over northern India,
6 the Himalayas and TP with the growth of topography for both uplift stages (Fig. 13). The
7 inverse relation between the enrichment in heavy isotopes in precipitation and
8 precipitation amount, named the “amount effect” (Dansgaard, 1964) is largely known for
9 oceanic tropical conditions (Risi et al., 2008; Rozanski, Kazimierz Araguás-Araguás and
10 Gonfiantini, 1993) and for Asia monsoonal areas (Lee et al., 2012; Yang et al., 2011).
11 Over South Tibet recent studies have shown the role of deep convection in isotopic
12 depletion (He et al., 2015). For the two stages of uplift, the residual component of the
13 isotopic signal depicts negative values over southern TP, where annual rainfall amount is
14 increased. Thus we infer that this anomaly can be driven, at least partly, by the amount
15 effect that increases with growing topography.

16 Various climate studies have suggested that the appearance of the monsoonal system in
17 East Asia and the onset of central Asian desertification were related to Cenozoic
18 Himalayan–Tibetan uplift and withdrawal of the Paratethys Sea (An et al., 2001; Clift et
19 al., 2008; Guo et al., 2002, 2008; Kutzbach et al., 1989, 1993; Ramstein et al., 1997;
20 Raymo and Ruddiman, 1992; Ruddiman and Kutzbach, 1989; Sun and Wang, 2005;
21 Zhang et al., 2007) although the exact timing of the monsoon onset and its intensification
22 remains debated (Licht et al., 2014; Molnar et al., 2010). Although our experimental
23 setup, which does not include Cenozoic paleogeography, was not designed to assess the
24 question of monsoon driving mechanisms nor its timing, our results suggest that uplifting
25 the Plateau from 250 meters ASL to half of its present height is enough to enhance
26 moisture transport towards northern India and strengthen seasonal rainfall. Nevertheless,
27 massive increase of rainfall over TP between INT and MOD experiments indicates that
28 the second phase of uplift might be crucial to activate an efficient, modern-day-like,
29 hydrological cycle over the Plateau. The decrease in simulated precipitation north of the
30 Plateau also suggests that terminal phase of TP uplift triggered modern-day arid areas.

31

1 **4.3 Other effects**

2 Although precipitation amount change explains well the residual isotopic anomaly (Fig.
3 10 F, Fig. 11 F), additional processes could interplay. Continental recycling can overprint
4 original moisture signature and shifts the isotopic ratios to higher values due to
5 recharging of moisture by heavy isotopes from soil evaporation (Lee et al., 2012; Risi et
6 al., 2013). In our simulation, we detect an increasing role of continental recycling in the
7 hydrological budget of the TP (Fig. S6), especially in its central part, that likely shifts the
8 $\delta^{18}\text{O}$ to more positive values and partially compensate for the depletion linked to the
9 “amount effect” over the central plateau. Another process frequently invoked to explain
10 the evolution of precipitation $\delta^{18}\text{O}$ patterns over TP is changes in moisture sources
11 (Bershaw et al., 2012; Dettman et al., 2003; Quade et al., 2007; Tian et al., 2007). Except
12 for the continentally recycled moisture, southern Himalayas precipitation moisture
13 originates mainly from the Indian, the Atlantic and the Pacific Oceans (Fig. S6).
14 Proximate oceanic basins are known to be sources of moisture with more positive
15 signature than remote ones (Chen et al., 2012; Gat, 1996). Supplemental analyses with
16 water-tagging feature of LMDZ-iso show that contribution of continental recycling to
17 rainfall over TP increases with the uplift, at the expense of Pacific and Indian sources
18 (Fig. S6). Although we have no mean to decipher between sources and amount effect in
19 the residual anomaly, it seems that the change of sources is not sufficient to yield a strong
20 offset of $\delta^{18}\text{O}$ values.

21

22 **4.4 Relevance of paleoelevation reconstructions based on paleo $\delta^{18}\text{O}$**

23 Quantitative paleoelevation reconstructions using modern altitude- $\delta^{18}\text{O}$ relationship will
24 succeed only if ΔR_p corresponds mainly to the direct topography effect. Modern
25 paleoaltimetry studies cover almost all regions of the Plateau for time periods ranging
26 from Palaeocene to Pleistocene-Quaternary (see data compilation in Caves et al., 2015).
27 Most of these studies consider changes in $\delta^{18}\text{O}$ as a direct effect of the topography uplift.
28 Paleoelevation studies locations (see Caves et al., 2015 for a synthesis) plotted over the
29 anomaly maps (Fig. 12 A, Fig. 13 A) show for what geographical regions restored
30 elevations should be used with an additional caution. Numerous paleoelevation data
31 points were located either over the northern part of the TP (from 34°N to 38°N and from
32 88°E to 100°E) or over the southern region (from 27°N to 33°N and from 75°E to 95°E).

1 Our model results show that when TP altitude is increased from half to full, considering
2 topography as an exclusive controlling factor of precipitation $\delta^{18}\text{O}$ over the southern
3 (northern) region likely yield overestimations (underestimations) of surface uplift, since
4 the topography effect is offset by RH and amount effects. Projecting our modelling
5 results to each locality where paleoelevation studies have been published (Table 4)
6 reveals that topography change explains simulated total isotopic change reasonably well
7 for only few locations (Linzhou Basin, Lunpola Basin, Kailas Basin, Huaitoutala).
8 Indeed topography appears to be the main controlling factor for only 40% of the sites,
9 while 30% are dominated by RH effects, 20% by residual effects and 5% and 5% by post-
10 condensational and non-adiabatic temperature changes, respectively. Nevertheless such
11 figures have to be taken carefully, since we ran idealized experiments testing only the
12 impact of uplift, neglecting other factors like horizontal paleogeography or pCO_2
13 variations, the latter being known to influence $\delta^{18}\text{O}$ as well (Jeffery et al., 2012; Poulsen
14 and Jeffery, 2011).

15 For the initial uplift stage apparent consistency occurs between the topography impact
16 and the total isotopic composition is observed, in relation with counteracting effects RH
17 and pots-condensational processes. For the southern region RH impact is appeared to be
18 the main controlling factor for the isotopic composition of precipitation, surpassing the
19 direct topography impact. Nevertheless, these processes have a different contribution for
20 initial and terminal stages of uplift. Precipitation changes lead to overestimate altitude
21 changes for both stages, but for the terminal stage its contribution is bigger. This effect
22 dominates in the southern part, and more generally where the isotopic composition of
23 precipitation strongly depends on convective activity. RH changes dominate over the
24 western part of TP and Northern India for initial uplift stage and over the northern TP for
25 the terminal. Differences between both stages could be partly explained by non-linearities
26 in qs-temperature relationships, as well as in Rayleigh distillation processes. Determining
27 whether other processes contribute to this difference would be of interest, but was out of
28 the scope of the present-study.

29

30 **5 Conclusions**

31 Previous studies focusing on the Andes (Ehlers and Poulsen, 2009; Poulsen et al., 2010)
32 or north American cordillera (Sewall and Fricke, 2013) have inferred that the impact of

1 uplift of mountain ranges on $\delta^{18}\text{O}$ could be altered by the consequences of the uplift on
2 atmospheric physics and dynamics. Our modelling results show that it is also the case for
3 the Tibetan Plateau uplift. Additionally, we designed a decomposing analysis to quantify
4 for the first time the different processes that can alter precipitation $\delta^{18}\text{O}$ changes with
5 uplift. As suggested for the Andes, the onset of convective rainfall plays an important
6 role in shifting $\delta^{18}\text{O}$ towards more negative values. Nevertheless this process is not the
7 main factor, as we show that saturation of air masses, quantified by RH have two to
8 three-time bigger effects on the final $\delta^{18}\text{O}$. We infer that increase in precipitation linked
9 with the TP uplift would lead to overestimation of the topography uplift at sites over
10 Himalayas and Southern TP, whereas increase in RH leads to underestimating the uplift
11 at sites in Northern Tibet.

12 Our results could be applied to interpret paleoclimate records and to reconstruct the
13 region uplift history. Paleoelevation reconstructions suggest the Himalayas attained their
14 current elevation by **at least by the late Miocene or even earlier** (Garzione et al., 2000a,
15 2000b; Rowley et al., 2001; Saylor et al., 2009). Our results show overestimation of the
16 topography impact over this region, thus the Himalayas may have attained their current
17 elevation later than expected. In contrast, isotope-based paleoaltimetry could
18 underestimate surface elevation over the northern TP. This could explain why available
19 isotope-based paleoelevation estimates for the northern TP (Cyr et al., 2005), which
20 estimates surface elevation about 2km, contradict palynological assemblages in lacustrine
21 sediments from the Xining **Basin**, which show the presence of high-altitude vegetation at
22 the same time period (Dupont-Nivet et al., 2008; Hoorn et al., 2012).

23 Still, our decomposition methods reveal that even if the impact of the TP uplift phases are
24 rather straightforward (monsoon enhancement to the South, increase in continental
25 recycling over TP, moisture fluxes deflection and increased aridity to the North), the
26 consequences in terms of $\delta^{18}\text{O}$ are extremely complex, since interplays and compensation
27 occur amongst all the processes. Limitations in our approach are related to **a perfectible
28 hydrological cycle in LMDZ-iso, and ~~the theoretical uplift scenario we chose~~ the idealized
29 boundary conditions (topography uplift scenarios, modern land-sea mask, SSTs and
30 $p\text{CO}_2$). Model-data comparison show that mean annual precipitation amount is slightly
31 overestimated by the model for the northern TP, thus could result in underestimation of
32 the amount effect contribution for the northern TP. On the contrary, the model**

1 overestimates the precipitation over the southern edge of Himalayas. If it was more
2 realistic, the contribution of the amount effect estimated by the decomposing method
3 could be less important. Changes in vegetation cover, by altering albedo and persistence
4 of snow cover, could affect the impact of non-adiabatic temperature changes on $\delta^{18}\text{O}$.
5 Vegetation over Asia was shown to have a major variation through Cenozoic based on
6 pollen (Dupont-Nivet et al., 2008; Miao et al., 2011; Song et al., 2010; Zhao and Yu,
7 2012) and paleobotanical data (An et al., 2005; De Franceschi et al., 2008; Kohn, 2010)
8 and future studies would benefit to explore its impact on precipitation $\delta^{18}\text{O}$. Also it is
9 largely known that during the Cenozoic air temperature was higher due to higher
10 concentration of greenhouse gases in the atmosphere (Zachos et al., 2008). Studies taking
11 into account this feedback inferred that it could lead to even larger inaccuracy in surface
12 uplift estimations during the Cenozoic (Poulsen and Jeffery, 2011). Thus the field of
13 paleoaltimetry would benefit from future studies focusing on (1) using paleoclimate
14 proxies to constrain specifically relative humidity, surface temperature and precipitation
15 amount in deep time and (2) applying a decomposition method to isotope-enabled GCM
16 simulations forced by constrained paleogeography (land-sea mask and different scenarios
17 for orogens) and atmospheric pCO_2 for specific geological time period. The combination
18 of both could help refining calibration for paleo $\delta^{18}\text{O}$ -elevation relationships and refining
19 paleoelevation estimates.

20

21 **Acknowledgements**

22 This work is a part of iTECC (interaction Tectonics-Erosion-Climate-Coupling) project
23 funded by European Union. Computational resources were provided by IDRIS-GENCI
24 (project 0292), France

25

26 **References**

27 An, Z., Kutzbach, J. E., Prell, W. L. and Porter, S. C.: Evolution of Asian monsoons and
28 phased uplift of the Himalaya-Tibetan plateau since Late Miocene times., *Nature*,
29 411(6833), 62–66, doi:10.1038/35075035, 2001.

30 An, Z., Huang, Y., Liu, W., Guo, Z., Stevens, C., Li, L., Prell, W., Ning, Y., Cai, Y.,
31 Zhou, W., Lin, B., Zhang, Q., Cao, Y., Qiang, X., Chang, H. and Wu, Z.: Multiple

1 expansions of C4 plant biomass in East Asia since 7 Ma coupled with strengthened
2 monsoon circulation, *Geology*, 33(9), 705, doi:10.1130/G21423.1, 2005.

3 An, Z., Wu, G., Li, J., Sun, Y., Liu, Y., Zhou, W., Cai, Y., Duan, A., Li, L., Mao, J.,
4 Cheng, H., Shi, Z., Tan, L., Yan, H., Ao, H., Chang, H. and Feng, J.: Global Monsoon
5 Dynamics and Climate Change, *Annu. Rev. Earth Planet. Sci.*, 43(1), 29–77,
6 doi:10.1146/annurev-earth-060313-054623, 2015.

7 Battisti, D. S., Ding, Q. and Roe, G. H.: Coherent pan-Asian climatic and isotopic
8 response to orbital forcing of tropical insolation, *J. Geophys. Res. Atmos.*, 119(21),
9 11997–12020, doi:10.1002/2014JD021960, 2014.

10 Bershaw, J., Penny, S. M. and Garzzone, C. N.: Stable isotopes of modern water across
11 the Himalaya and eastern Tibetan Plateau: Implications for estimates of paleoelevation
12 and paleoclimate, *J. Geophys. Res. Atmos.*, 117(2), 1–18, doi:10.1029/2011JD016132,
13 2012.

14 Boos, W. R. (yale): A review of recent progress on Tibet’s role in the South Asian
15 monsoon, *Clivar*, (1996), 2015.

16 Broccoli, A. J. and Manabe, S.: The Effects of Orography on Midlatitude Northern
17 Hemisphere Dry Climates, *J. Clim.*, 5(11), 1181–1201, doi:10.1175/1520-
18 0442(1992)005<1181:teoom>2.0.co;2, 1992.

19 Caves, J. K., Winnick, M. J., Graham, S. A., Sjostrom, D. J., Mulch, A. and Chamberlain,
20 C. P.: Role of the westerlies in Central Asia climate over the Cenozoic, *Earth Planet. Sci.*
21 *Lett.*, 428, 33–43, 2015.

22 Chen, B., Xu, X. De, Yang, S. and Zhang, W.: On the origin and destination of
23 atmospheric moisture and air mass over the Tibetan Plateau, *Theor. Appl. Climatol.*,
24 110(3), 423–435, doi:10.1007/s00704-012-0641-y, 2012.

25 Chen, G.-S., Liu, Z. and Kutzbach, J. E.: Reexamining the barrier effect of the Tibetan
26 Plateau on the South Asian summer monsoon, *Clim. Past*, 10(3), 1269–1275,
27 doi:10.5194/cp-10-1269-2014, 2014.

28 Clift, P. D., Hodges, K. V., Heslop, D., Hannigan, R., Van Long, H. and Calves, G.:
29 Correlation of Himalayan exhumation rates and Asian monsoon intensity, *Nat. Geosci.*,
30 1(12), 875–880, doi:10.1038/ngeo351, 2008.

1 Currie, B. S., Rowley, D. B. and Tabor, N. J.: Middle Miocene paleoaltimetry of southern
2 Tibet: Implications for the role of mantle thickening and delamination in the Himalayan
3 orogen, *Geology*, 33(3), 181–184, doi:10.1130/G21170.1, 2005.

4 Cyr, A. J., Currie, B. S. and Rowley, D. B.: Geochemical Evaluation of Fenghuoshan
5 Group Lacustrine Carbonates, North-Central Tibet: Implications for the Paleoaltimetry of
6 the Eocene Tibetan Plateau, *J. Geol.*, 113(5), 517–533, doi:10.1086/431907, 2005.

7 Dansgaard, W.: Stable isotopes in precipitation, *Tellus A*,
8 doi:10.3402/tellusa.v16i4.8993, 1964.

9 DeCelles, P. G., Quade, J., Kapp, P., Fan, M., Dettman, D. L. and Ding, L.: High and dry
10 in central Tibet during the Late Oligocene, *Earth Planet. Sci. Lett.*, 253(3-4), 389–401,
11 doi:10.1016/j.epsl.2006.11.001, 2007.

12 Dettman, D. L., Fang, X., Garzzone, C. N. and Li, J.: Uplift-driven climate change at 12
13 Ma: A long $\delta^{18}\text{O}$ record from the NE margin of the Tibetan plateau, *Earth Planet. Sci.*
14 *Lett.*, 214(1-2), 267–277, doi:10.1016/S0012-821X(03)00383-2, 2003.

15 Ding, L., Xu, Q., Yue, Y., Wang, H., Cai, F. and Li, S.: The Andean-type Gangdese
16 Mountains: Paleoelevation record from the Paleocene-Eocene Linzhou Basin, *Earth*
17 *Planet. Sci. Lett.*, 392, 250–264, doi:10.1016/j.epsl.2014.01.045, 2014.

18 Dupont-Nivet, G., Hoom, C. and Konert, M.: Tibetan uplift prior to the Eocene-
19 Oligocene climate transition: Evidence from pollen analysis of the Xining Basin,
20 *Geology*, 36(12), 987–990, doi:10.1130/G25063A.1, 2008.

21 Ehlers, T. A. and Poulsen, C. J.: Influence of Andean uplift on climate and paleoaltimetry
22 estimates, *Earth Planet. Sci. Lett.*, 281(3-4), 238–248, doi:10.1016/j.epsl.2009.02.026,
23 2009.

24 Forest, C. E., Wolfe, J. A., Molnar, P. and Emanuel, K. A.: Paleoaltimetry incorporating
25 atmospheric physics and botanical estimates of paleoclimate, *Geol. Soc. Am. Bull.*,
26 111(4), 497–511, doi:10.1130/0016-7606(1999)111<0497:PIAPAB>2.3.CO;2, 1999.

27 De Franceschi, D., Hoorn, C., Antoine, P. O., Cheema, I. U., Flynn, L. J., Lindsay, E. H.,
28 Marivaux, L., Métais, G., Rajpar, A. R. and Welcomme, J. L.: Floral data from the mid-
29 Cenozoic of central Pakistan, *Rev. Palaeobot. Palynol.*, 150, 115–129,
30 doi:10.1016/j.revpalbo.2008.01.011, 2008.

1 Frankenberg, C., Yoshimura, K., Warneke, T., Aben, I., Butz, A., Deutscher, N., Griffith,
2 D., Hase, F., Notholt, J., Schneider, M., Schrijver, H. and Röckmann, T.: Dynamic
3 Processes Governing Lower-Tropospheric HDO/H₂O Ratios as Observed from Space and
4 Ground, *Science* (80-.), 325(5946), 1374–1377, doi:10.1126/science.1173791, 2009.

5 Galewsky, J. and Hurley, J. V: An advection-condensation model for subtropical water
6 vapor isotopic ratios, *J. Geophys. Res. Atmos.*, 115(D16), 2010.

7 Galewsky, J., Sobel, A. and Held, I.: Diagnosis of subtropical humidity dynamics using
8 tracers of last saturation, *J. Atmos. Sci.*, 62(9), 3353–3367, 2005.

9 Garzione, C. N., Dettman, D. L., Quade, J., De Celles, P. G. and Butler, R. F.: High times
10 on the Tibetan Plateau: Paleoelevation of the Thakkhola graben, Nepal, *Geology*, 28(4),
11 339–342, doi:10.1130/0091-7613(2000)28<339:HTOTTP>2.0.CO;2, 2000a.

12 Garzione, C. N., Quade, J., DeCelles, P. G. and English, N. B.: Predicting paleoelevation
13 of Tibet and the Himalaya from $\delta^{18}\text{O}$ vs. altitude gradients in meteoric water across the
14 Nepal Himalaya, *Earth Planet. Sci. Lett.*, 183(1-2), 215–229, doi:10.1016/S0012-
15 821X(00)00252-1, 2000b.

16 Gat, J. R.: Oxygen and hydrogen isotopes in the hydrologic cycle, *Annu. Rev. Earth*
17 *Planet. Sci.*, 24(1), 225–262, 1996.

18 Gedzelman, S. D. and Arnold, R.: Modeling the isotopic composition of precipitation,
19 New York, 99, 1994.

20 Gonfiantini, R., Roche, M. A., Olivry, J. C., Fontes, J. C. and Zuppi, G. M.: The altitude
21 effect on the isotopic composition of tropical rains, *Chem. Geol.*, 181(1-4), 147–167,
22 doi:10.1016/S0009-2541(01)00279-0, 2001.

23 Guo, Z. T., Ruddiman, W. F., Hao, Q. Z., Wu, H. B., Qiao, Y. S., Zhu, R. X., Peng, S. Z.,
24 Wei, J. J., Yuan, B. Y. and Liu, T. S.: Onset of Asian desertification by 22 Myr ago
25 inferred from loess deposits in China., *Nature*, 416(6877), 159–163,
26 doi:10.1038/416159a, 2002.

27 Guo, Z. T., Sun, B., Zhang, Z. S., Peng, S. Z., Xiao, G. Q., Ge, J. Y., Hao, Q. Z., Qiao, Y.
28 S., Liang, M. Y., Liu, J. F., Yin, Q. Z. and Wei, J. J.: A major reorganization of Asian
29 climate by the early Miocene, *Clim. Past*, 4(3), 153–174, doi:10.5194/cp-4-153-2008,
30 2008.

1 Harris, N.: The elevation history of the Tibetan Plateau and its implications for the Asian
2 monsoon, *Palaeogeogr. Palaeoclimatol. Palaeoecol.*, 241(1), 4–15,
3 doi:10.1016/j.palaeo.2006.07.009, 2006a.

4 Harris, N.: The elevation history of the Tibetan Plateau and its implications for the Asian
5 monsoon, *Palaeogeogr. Palaeoclimatol. Palaeoecol.*, 241(1), 4–15,
6 doi:10.1016/j.palaeo.2006.07.009, 2006b.

7 He, Y., Risi, C., Gao, J., Masson-delmotte, V., Yao, T., Lai, C., Ding, Y., Worden, J.,
8 Frankenberg, C., Chepfer, H. and Cesana, G.: Special Section : Impact of atmospheric
9 convection on south Tibet summer precipitation isotopologue composition using a
10 combination of in situ measurements, satellite data, and atmospheric general circulation
11 modeling, , 3852–3871, doi:10.1002/2014JD022180.Abstract, 2015.

12 Hoke, G. D., Liu-Zeng, J., Hren, M. T., Wissink, G. K. and Garziona, C. N.: Stable
13 isotopes reveal high southeast Tibetan Plateau margin since the Paleogene, *Earth Planet.
14 Sci. Lett.*, 394, 270–278, doi:10.1016/j.epsl.2014.03.007, 2014.

15 Hoorn, C., Straathof, J., Abels, H. a., Xu, Y., Utescher, T. and Dupont-Nivet, G.: A late
16 Eocene palynological record of climate change and Tibetan Plateau uplift (Xining Basin,
17 China), *Palaeogeogr. Palaeoclimatol. Palaeoecol.*, 344-345, 16–38,
18 doi:10.1016/j.palaeo.2012.05.011, 2012.

19 Hourdin, F., Musat, I., Bony, S., Braconnot, P., Codron, F., Dufresne, J. L., Fairhead, L.,
20 Filiberti, M. A., Friedlingstein, P., Grandpeix, J. Y., Krinner, G., LeVan, P., Li, Z. X. and
21 Lott, F.: The LMDZ4 general circulation model: Climate performance and sensitivity to
22 parametrized physics with emphasis on tropical convection, *Clim. Dyn.*, 27(7-8), 787–
23 813, doi:10.1007/s00382-006-0158-0, 2006.

24 Hren, M. T., Bookhagen, B., Blisniuk, P. M., Booth, A. L. and Chamberlain, C. P.: $\delta^{18}\text{O}$
25 and δD of streamwaters across the Himalaya and Tibetan Plateau: Implications for
26 moisture sources and paleoelevation reconstructions, *Earth Planet. Sci. Lett.*, 288(1-2),
27 20–32, doi:10.1016/j.epsl.2009.08.041, 2009.

28 Jeffery, M. L., Poulsen, C. J. and Ehlers, T. A.: Impacts of Cenozoic global cooling,
29 surface uplift, and an inland seaway on South American paleoclimate and precipitation
30 $\delta^{18}\text{O}$, *Geol. Soc. Am. Bull.*, 124(3-4), 335–351, 2012.

31 Kageyama, M., Nebout, N. C., Sepulchre, P., Peyron, O., Krinner, G., Ramstein, G. and

1 Cazet, J.-P.: The Last Glacial Maximum and Heinrich Event 1 in terms of climate and
2 vegetation around the Alboran Sea: a preliminary model-data comparison, *Comptes*
3 *Rendus Geosci.*, 337(10-11), 983–992, doi:10.1016/j.crte.2005.04.012, 2005.

4 Kanamitsu, M., Ebisuzaki, W., Woollen, J., Yang, S. K., Hnilo, J. J., Fiorino, M. and
5 Potter, G. L.: NCEP-DOE AMIP-II reanalysis (R-2), *Bull. Am. Meteorol. Soc.*, 83(11),
6 1631–1643+1559, doi:10.1175/BAMS-83-11-1631, 2002.

7 Kattel, D. B., Yao, T., Yang, W., Gao, Y. and Tian, L.: Comparison of temperature lapse
8 rates from the northern to the southern slopes of the Himalayas, *Int. J. Climatol.*, 2015.

9 Khan, M. A., Spicer, R. a., Bera, S., Ghosh, R., Yang, J., Spicer, T. E. V, Guo, S. X., Su,
10 T., Jacques, F. and Grote, P. J.: Miocene to Pleistocene floras and climate of the Eastern
11 Himalayan Siwaliks, and new palaeoelevation estimates for the Namling-Oiyug Basin,
12 Tibet, *Glob. Planet. Change*, 113, 1–10, doi:10.1016/j.gloplacha.2013.12.003, 2014.

13 Kohn, M. J.: Carbon isotope compositions of terrestrial C3 plants as indicators of
14 (paleo)ecology and (paleo)climate, *Proc. Natl. Acad. Sci.*, 107(46), 19691–19695,
15 doi:10.1073/pnas.1004933107, 2010.

16 Kutzbach, J. E., Guetter, P. J., Ruddiman, W. F. and Prell, W. L.: Sensitivity of climate to
17 late Cenozoic uplift in southern Asia and the American west: numerical experiments, *J.*
18 *Geophys. Res. Atmos.*, 94(D15), 18393–18407, 1989.

19 Kutzbach, J. E., Prell, W. L. and Ruddiman, W. F.: Sensitivity of Eurasian climate to
20 surface uplift of the Tibetan Plateau, *J. Geol.*, 177–190, 1993.

21 Ladant, J., Donnadiou, Y., Lefebvre, V. and Dumas, C.: The respective role of
22 atmospheric carbon dioxide and orbital parameters on ice sheet evolution at the Eocene-
23 Oligocene transition, *Paleoceanography*, 29(8), 810–823, doi:10.1002/2013PA002593,
24 2014.

25 Lee, J. and Fung, I.: “Amount effect” of water isotopes and quantitative analysis of post-
26 condensation processes, *Hydrol. Process.*, 22(1), 1–8, 2008.

27 Lee, J. E., Risi, C., Fung, I., Worden, J., Scheepmaker, R. A., Lintner, B. and
28 Frankenberg, C.: Asian monsoon hydrometeorology from TES and SCIAMACHY water
29 vapor isotope measurements and LMDZ simulations: Implications for speleothem climate
30 record interpretation, *J. Geophys. Res. Atmos.*, 117(15), 1–12,

1 doi:10.1029/2011JD017133, 2012.

2 Van Leer, B.: Towards the ultimate conservative difference scheme. IV. A new approach
3 to numerical convection, *J. Comput. Phys.*, 23(3), 276–299,
4 doi:http://dx.doi.org/10.1016/0021-9991(77)90095-X, 1977.

5 LeGrande, A. N. and Schmidt, G. A.: Sources of Holocene variability of oxygen isotopes
6 in paleoclimate archives, *Clim. Past*, 5(3), 441–455, doi:10.5194/cp-5-441-2009, 2009.

7 Li, S., Currie, B. S., Rowley, D. B. and Ingalls, M.: Cenozoic paleoaltimetry of the SE
8 margin of the Tibetan Plateau: Constraints on the tectonic evolution of the region, *Earth
9 Planet. Sci. Lett.*, 432, 415–424, doi:10.1016/j.epsl.2015.09.044, 2015.

10 Licht, A., van Cappelle, M., Abels, H. A., Ladant, J.-B., Trabucho-Alexandre, J., France-
11 Lanord, C., Donnadieu, Y., Vandenberghe, J., Rigaudier, T., Lécuyer, C., Terry Jr, D.,
12 Adriaens, R., Boura, A., Guo, Z., Soe, A. N., Quade, J., Dupont-Nivet, G. and Jaeger, J.-
13 J.: Asian monsoons in a late Eocene greenhouse world, *Nature*, 513(7519), 501–506,
14 doi:10.1038/nature13704, 2014.

15 Liu, X., Sun, H., Miao, Y., Dong, B. and Yin, Z.-Y.: Impacts of uplift of northern Tibetan
16 Plateau and formation of Asian inland deserts on regional climate and environment, *Quat.
17 Sci. Rev.*, 116, 1–14, doi:10.1016/j.quascirev.2015.03.010, 2015.

18 McElwain, J. C.: Climate-independent paleoaltimetry using stomatal density in fossil
19 leaves as a proxy for CO₂ partial pressure, *Geology*, 32(12), 1017,
20 doi:10.1130/G20915.1, 2004.

21 Merlivat, L. and Nief, G.: Fractionnement isotopique lors des changements d'état solide-
22 vapeur et liquide-vapeur de l'eau à des températures inférieures à 0°C, *Tellus*, 19(1), 122–
23 127, doi:10.1111/j.2153-3490.1967.tb01465.x, 1967.

24 Miao, Y., Fang, X., Herrmann, M., Wu, F., Zhang, Y. and Liu, D.: Miocene pollen record
25 of KC-1 core in the Qaidam Basin, NE Tibetan Plateau and implications for evolution of
26 the East Asian monsoon, *Palaeogeogr. Palaeoclimatol. Palaeoecol.*, 299(1-2), 30–38,
27 doi:10.1016/j.palaeo.2010.10.026, 2011.

28 Miao, Y., Herrmann, M., Wu, F., Yan, X. and Yang, S.: What controlled Mid-Late
29 Miocene long-term aridification in Central Asia? - Global cooling or Tibetan Plateau
30 uplift: A review, *Earth-Science Rev.*, 112(3-4), 155–172,

1 doi:10.1016/j.earscirev.2012.02.003, 2012.

2 Molnar, P., Boos, W. R. and Battisti, D. S.: Orographic Controls on Climate and
3 Paleoclimate of Asia: Thermal and Mechanical Roles for the Tibetan Plateau, *Annu. Rev.*
4 *Earth Planet. Sci.*, 38(1), 77–102, doi:10.1146/annurev-earth-040809-152456, 2010.

5 Mulch, A.: Stable isotope paleoaltimetry and the evolution of landscapes and life, *Earth*
6 *Planet. Sci. Lett.*, 433, 180–191, doi:10.1016/j.epsl.2015.10.034, 2016.

7 New, M., Lister, D., Hulme, M. and Makin, I.: A high-resolution data set of surface
8 climate over global land areas, *Clim. Res.*, 21(1), 1–25, doi:10.3354/cr021001, 2002.

9 Pausata, F. S. R., Battisti, D. S., Nisancioglu, K. H. and Bitz, C. M.: Chinese stalagmite
10 $\delta^{18}\text{O}$ controlled by changes in the Indian monsoon during a simulated Heinrich event,
11 *Nat. Geosci.*, 4(7), 474–480, doi:10.1038/ngeo1169, 2011.

12 Poage, M. A. and Chamberlain, C. P.: Empirical relationships between elevation and the
13 stable isotope composition of precipitation and surface waters: Considerations for studies
14 of paleoelevation change, *Am. J. Sci.*, 301(1), 1–15, doi:10.2475/ajs.301.1.1, 2001.

15 Pohl, A., Donnadieu, Y., Le Hir, G., Buoncristiani, J.-F. and Vennin, E.: Effect of the
16 Ordovician paleogeography on the (in)stability of the climate, *Clim. Past*, 10(6), 2053–
17 2066, doi:10.5194/cp-10-2053-2014, 2014.

18 Poulsen, C. J. and Jeffery, M. L.: Climate change imprinting on stable isotopic
19 compositions of high-elevation meteoric water cloaks past surface elevations of major
20 orogens, *Geology*, 39(6), 595–598, doi:10.1130/G32052.1, 2011.

21 Poulsen, C. J., Ehlers, T. a and Insel, N.: Onset of convective rainfall during gradual late
22 Miocene rise of the central Andes., *Science*, 328(5977), 490–493,
23 doi:10.1126/science.1185078, 2010.

24 Quade, J., Garzzone, C. and Eiler, J.: Paleoelevation Reconstruction using Pedogenic
25 Carbonates, *Rev. Mineral. Geochemistry*, 66(1), 53–87, doi:10.2138/rmg.2007.66.3,
26 2007.

27 Quade, J., Breecker, D. O., Daëron, M. and Eiler, J.: The paleoaltimetry of Tibet: An
28 isotopic perspective, *Am. J. Sci.*, 311(2), 77–115, doi:10.2475/02.2011.01, 2011.

29 Ramstein, G., Fluteau, F., Besse, J. and Jousaume, S.: Effect of orogeny, plate motion
30 and land–sea distribution on Eurasian climate change over the past 30 million years,

- 1 Nature, 386(6627), 788–795, doi:10.1038/386788a0, 1997.
- 2 Raymo, M. E. and Ruddiman, W. F.: Tectonic forcing of late Cenozoic climate, Nature,
3 359(6391), 117–122, 1992.
- 4 Risi, C., Bony, S. and Vimeux, F.: Influence of convective processes on the isotopic
5 composition ($\delta^{18}\text{O}$ and δD) of precipitation and water vapor in the tropics: 2. Physical
6 interpretation of the amount effect, J. Geophys. Res. Atmos., 113(19), 1–12,
7 doi:10.1029/2008JD009943, 2008.
- 8 Risi, C., Bony, S., Vimeux, F. and Jouzel, J.: Water-stable isotopes in the LMDZ4
9 general circulation model: Model evaluation for present-day and past climates and
10 applications to climatic interpretations of tropical isotopic records, J. Geophys. Res.
11 Atmos., 115(12), 1–27, doi:10.1029/2009JD013255, 2010.
- 12 Risi, C., Noone, D., Frankenberg, C. and Worden, J.: Role of continental recycling in
13 intraseasonal variations of continental moisture as deduced from model simulations and
14 water vapor isotopic measurements, Water Resour. Res., 49(7), 4136–4156,
15 doi:10.1002/wrcr.20312, 2013.
- 16 Rodwell, M. J. and Hoskins, B. J.: Subtropical anticyclones and summer monsoons, J.
17 Clim., 14(15), 3192–3211, 2001.
- 18 Rowley, D. B. and Currie, B. S.: Palaeo-altimetry of the late Eocene to Miocene Lunpola
19 basin, central Tibet., Nature, 439(7077), 677–681, doi:10.1038/nature04506, 2006.
- 20 Rowley, D. B. and Garzzone, C. N.: Stable Isotope-Based Paleoaltimetry, Annu. Rev.
21 Earth Planet. Sci., 35(1), 463–508, doi:10.1146/annurev.earth.35.031306.140155, 2007.
- 22 Rowley, D. B., Pierrehumbert, R. T. and Currie, B. S.: A new approach to stable isotope-
23 based paleoaltimetry: Implications for paleoaltimetry and paleohypsometry of the High
24 Himalaya since the late Miocene, Earth Planet. Sci. Lett., 188(1-2), 253–268,
25 doi:10.1016/S0012-821X(01)00324-7, 2001.
- 26 Royden, L. H., Burchfiel, B. C. and Hilst, R. D. Van Der: The Geological Evolution of
27 the Tibetan Plateau, , 321(August), 1054–1058, 2008.
- 28 Rozanski, Kazimierz Araguás-Araguás, L. and Gonfiantini, R.: Isotopic patterns in
29 modern global precipitation, Clim. Chang. Cont. Isot. Rec., 1–36, 1993.
- 30 Ruddiman, W. F. and Kutzbach, J. E.: Forcing of late Cenozoic northern hemisphere

1 climate by plateau uplift in southern Asia and the American West, *J. Geophys. Res.*
2 *Atmos.*, 94(D15), 18409–18427, 1989.

3 Sato, T. and Kimura, F.: Impact of diabatic heating over the Tibetan Plateau on
4 subsidence over northeast Asian arid region, *Geophys. Res. Lett.*, 32(5), 1–5,
5 doi:10.1029/2004GL022089, 2005.

6 Saylor, J. E., Quade, J., Dettman, D. L., DeCelles, P. G., Kapp, P. A. and Ding, L.: The
7 late Miocene through present paleoelevation history of southwestern Tibet, *Am. J. Sci.*,
8 309(1), 1–42, doi:10.2475/01.2009.01, 2009.

9 Sepulchre, P., Ramstein, G., Fluteau, F., Schuster, M., Tiercelin, J.-J. and Brunet, M.:
10 Tectonic uplift and Eastern Africa aridification., *Science*, 313(5792), 1419–1423,
11 doi:10.1126/science.1129158, 2006.

12 Sewall, J. O. and Fricke, H. C.: Andean-scale highlands in the Late Cretaceous Cordillera
13 of the North American western margin, *Earth Planet. Sci. Lett.*, 362, 88–98,
14 doi:10.1016/j.epsl.2012.12.002, 2013.

15 Sherwood, S. C.: Maintenance of the free-tropospheric tropical water vapor distribution.
16 Part II: Simulation by large-scale advection, *J. Clim.*, 9(11), 2919–2934, 1996.

17 Song, X. Y., Spicer, R. a., Yang, J., Yao, Y. F. and Li, C. Sen: Pollen evidence for an
18 Eocene to Miocene elevation of central southern Tibet predating the rise of the High
19 Himalaya, *Palaeogeogr. Palaeoclimatol. Palaeoecol.*, 297(1), 159–168,
20 doi:10.1016/j.palaeo.2010.07.025, 2010.

21 Stowhas, L. and Moyano, J. C.: Simulation of the Isotopic Content of Precipitation,
22 *Atmos. Environ. Part a-General Top.*, 27(3), 327–333, doi:10.1016/0960-1686(93)90106-
23 9, 1993.

24 Sun, B., Wang, Y.-F., Li, C.-S., Yang, J., Li, J.-F., Li, Y.-L., Deng, T., Wang, S.-Q.,
25 Zhao, M., Spicer, R. a., Ferguson, D. K. and Mehrotra, R. C.: Early Miocene elevation in
26 northern Tibet estimated by palaeobotanical evidence, *Sci. Rep.*, 5(1), 10379,
27 doi:10.1038/srep10379, 2015.

28 Sun, J., Zhang, Z. and Zhang, L.: New evidence on the age of the Taklimakan Desert,
29 *Geology*, 37(2), 159–162, doi:10.1130/G25338A.1, 2009.

30 Sun, J., Xu, Q., Liu, W., Zhang, Z., Xue, L. and Zhao, P.: Palynological evidence for the

- 1 latest Oligocene-early Miocene paleoelevation estimate in the Lunpola Basin, central
2 Tibet, *Palaeogeogr. Palaeoclimatol. Palaeoecol.*, 399, 21–30,
3 doi:10.1016/j.palaeo.2014.02.004, 2014.
- 4 Sun, X. and Wang, P.: How old is the Asian monsoon system?—Palaeobotanical records
5 from China, *Palaeogeogr. Palaeoclimatol. Palaeoecol.*, 222(3–4), 181–222,
6 doi:http://dx.doi.org/10.1016/j.palaeo.2005.03.005, 2005.
- 7 Tapponnier, P., Zhiqin, X., Roger, F., Meyer, B., Arnaud, N., Wittlinger, G. and Jingsui,
8 Y.: Oblique stepwise rise and growth of the Tibet plateau., *Science*, 294(5547), 1671–
9 1677, doi:10.1126/science.105978, 2001.
- 10 Taylor, K. E., Williamson, D. and Zwiers, F.: The sea surface temperature and sea-ice
11 concentration boundary conditions for AMIP II simulations, Program for Climate Model
12 Diagnosis and Intercomparison, Lawrence Livermore National Laboratory, University of
13 California., 2000.
- 14 Tian, L., Yao, T., MacClune, K., White, J. W. C., Schilla, A., Vaughn, B., Vachon, R.
15 and Ichiyanagi, K.: Stable isotopic variations in west China: A consideration of moisture
16 sources, *J. Geophys. Res. Atmos.*, 112(10), 1–12, doi:10.1029/2006JD007718, 2007.
- 17 Vuille, M., Werner, M., Bradley, R. S., Chan, R. Y. and Keimig, F.: Stable isotopes in
18 East African precipitation record Indian Ocean zonal mode, *Geophys. Res. Lett.*, 32(21),
19 1–5, doi:10.1029/2005GL023876, 2005.
- 20 Xu, Q., Ding, L., Zhang, L., Cai, F., Lai, Q., Yang, D. and Liu-Zeng, J.: Paleogene high
21 elevations in the Qiangtang Terrane, central Tibetan Plateau, *Earth Planet. Sci. Lett.*, 362,
22 31–42, doi:10.1016/j.epsl.2012.11.058, 2013.
- 23 Yang, X., Yao, T., Yang, W., Yu, W. and Qu, D.: Co-existence of temperature and
24 amount effects on precipitation $\delta^{18}\text{O}$ in the Asian monsoon region, *Geophys. Res. Lett.*,
25 38(November), 1–6, doi:10.1029/2011GL049353, 2011.
- 26 Yao, T., Masson-Delmotte, V., Gao, J., Yu, W., Yang, X., Risi, C., Sturm, C., Werner,
27 M., Zhao, H., He, Y., Ren, W., Tian, L., Shi, C. and Hou, S.: A review of climatic
28 controls on $\delta^{18}\text{O}$ in precipitation over the Tibetan Plateau: Observations and simulations,
29 *Rev. Geophys.*, 51(4), 525–548, doi:10.1002/rog.20023, 2013.
- 30 Zachos, J. C., Dickens, G. R. and Zeebe, R. E.: An early Cenozoic perspective on

1 greenhouse warming and carbon-cycle dynamics., *Nature*, 451(7176), 279–283,
2 doi:10.1038/nature06588, 2008.

3 Zhang, R., Jiang, D., Zhang, Z. and Yu, E.: The impact of regional uplift of the Tibetan
4 Plateau on the Asian monsoon climate, *Palaeogeogr. Palaeoclimatol. Palaeoecol.*, 417,
5 137–150, doi:10.1016/j.palaeo.2014.10.030, 2015.

6 Zhang, Z., Wang, H., Guo, Z. and Jiang, D.: What triggers the transition of
7 palaeoenvironmental patterns in China, the Tibetan Plateau uplift or the Paratethys Sea
8 retreat?, *Palaeogeogr. Palaeoclimatol. Palaeoecol.*, 245(3-4), 317–331,
9 doi:10.1016/j.palaeo.2006.08.003, 2007.

10 Zhao, Y. and Yu, Z.: Vegetation response to Holocene climate change in East Asian
11 monsoon-margin region, *Earth-Science Rev.*, 113(1-2), 1–10,
12 doi:10.1016/j.earscirev.2012.03.001, 2012.

13

14

15

16

17

18

19

20

21

22

23

24

25

26

27

1 Table 1. Table detailing how the different terms of the decomposition for ΔR_p , as written
 2 in Eq. (7), are estimated

3

Term written with differential format	Estimate of these terms	Physical meaning
ΔR_p	$R_p(\delta R_{vi2}, \varepsilon_2, h_2, \delta T_{s2}, z_2) - R_p(\delta R_{vi1}, \varepsilon_1, h_1, \delta T_{s1}, z_1)$	Total isotopic difference between state 1 and state 2
$\Delta R_{p,\Delta z}$	$R_p(\varepsilon', \delta R_v', h', \delta T_s', z_2) - R_p(\varepsilon', \delta R_v', h', \delta T_s', z_1)$	Direct effect of topography change
$\Delta R_{p,\Delta \delta T_s}$	$R_p(\varepsilon', \delta R_v', h', \delta T_{s2}, z') - R_p(\varepsilon', \delta R_v', h', \delta T_{s1}, z')$	Effect of lapse rate change, associated with non-adiabatic effects, possibly due to changes in surface energy budget or in large-scale atmospheric stratification
$\Delta R_{p,\Delta h}$	$R_p(\varepsilon', \delta R_v', h_2, \delta T_s', z') - R_p(\varepsilon', \delta R_v', h_1, \delta T_s', z')$	Effect of local relative humidity change, possibly due to large-scale circulation changes
$\Delta R_{p,\Delta \varepsilon}$	$R_p(\varepsilon_2, \delta R_v', h', \delta T_s', z') - R_p(\varepsilon_1, \delta R_v', h', \delta T_s', z')$	Effect of changes in condensational and post-condensational effects, possibly due to changes in rain reevaporation processes
$\Delta R_{p,\Delta \delta R_v}$	$R_p(\varepsilon', \delta R_{v2}, h', \delta T_s', z') - R_p(\varepsilon', \delta R_{v1}, h', \delta T_s', z')$	All other effects, including effects of deep convection, mixing, water vapour origin, continental recycling on the initial water vapour

4

1 Table 2. INT-LOW and MOD-INT sensitivity of the decomposition terms (in %) to the
 2 changes of R_{v0} , T_0 , q_0 , of 1%, 1K and 10% respectively.

3

	Northern Region			South region		
	T_0	q_0	R_{v0}	T_0	q_0	R_{v0}
INT-LOW experiment						
$\Delta R_{p,\Delta z}$	0.08	0.33	0.67	0.07	0.25	0.51
$\Delta R_{p,\Delta\delta T_s}$	0.01	0.02	0.04	0.07	0.06	0.13
$\Delta R_{p,\Delta h}$	0	0.35	0.66	0	0.19	0.83
$\Delta R_{p,\Delta\delta R_{vi}}$	0	0	0.05	0	0	0.52
$\Delta R_{p,\Delta\varepsilon}$	0	0	0	0	0	0
MOD-INT experiment						
$\Delta R_{p,\Delta z}$	0.21	0.6	0.8	0.17	0.59	0.9
$\Delta R_{p,\Delta\delta T_s}$	0.2	0.09	0.18	0.19	0.02	0.05
$\Delta R_{p,\Delta h}$	0	0.58	0.6	0	0.37	0.27
$\Delta R_{p,\Delta\delta R_{vi}}$	0	0	0.65	0	0	0.67
$\Delta R_{p,\Delta\varepsilon}$	0	0	0	0	0	0

4

5

6

7

8

9

1 Table 3. Values of isotopic changes due to decomposed terms for two uplift stages and
 2 for two regions (see the text)

Term	Isotopic change (‰)			
	Initial Stage		Terminal Stage	
	South	North	South	North
$\Delta R_{p,\Delta z}$	-1.40	-2.00	-3.96	-5.50
$\Delta R_{p,\Delta \delta T_s}$	0.4	-0.09	0.76	-0.25
$\Delta R_{p,\Delta h}$	2.40	1.97	1.38	2.50
$\Delta R_{p,\Delta \varepsilon}$	-1.30	-1.73	-0.41	0.01
$\Delta R_{p,\Delta \delta R_v}$	-1.10	-0.14	-2.38	-0.54
Total ΔR_p	-1.00	-1.99	-4.61	-3.16

3

4

5

1 Table 4. Impact of the different terms of the decomposition on the isotopic signal for the terminal stage of HTP uplift in the location where
 2 paleoelevation studies have been done

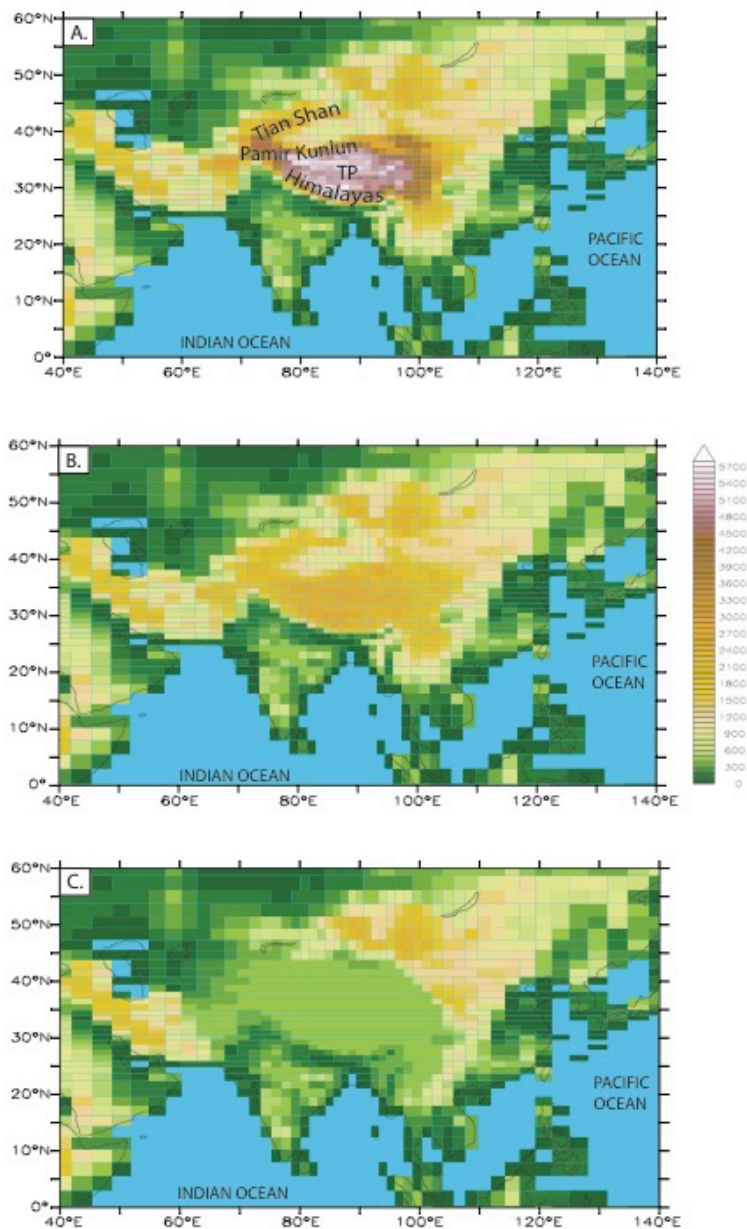
Locality	Latitude	Longitude	ΔR_p (‰)	$\Delta R_{p,\Delta z}$ (‰)	$\Delta R_{p,\Delta \delta T_s}$ (‰)	$\Delta R_{p,\Delta \varepsilon}$ (‰)	$\Delta R_{p,\Delta h}$ (‰)	$\Delta R_{p,\Delta \delta R_v}$ (‰)	Paleoelevation studies at this locality
Aertashi	37.97	75.55	-1.619	-2.859	0.999	-0.294	-0.268	0.803	Kent-Corson et al. (2009)
Biger Noor	45.90	96.78	-1.169	-0.004	2.673	-0.702	-4.419	1.283	Caves et al. (2014)
Chake Basin	23.80	103.10	-0.252	0.006	-0.030	0.042	0.263	-0.533	Hoke et al. (2014)
Dzereg	47.14	93.06	-1.006	-0.004	2.216	-0.372	-4.313	1.466	Caves et al. (2014)
Eryuan	26.20	99.80	-1.356	-1.574	0.634	0.171	0.497	-1.083	Hoke et al. (2014)
Ganchaigou	37.69	91.04	-3.195	-2.780	0.836	-1.292	0.610	-0.570	Kent-Corson et al. (2009)
Gyirong Basin	28.70	85.25	-7.017	-3.850	1.073	-1.089	0.409	-3.559	Wang et al. (1996)
Hexi Corridor	39.52	97.52	-2.907	-0.279	1.732	-1.985	-2.293	-0.083	Kent-Corson et al. (2009)
Hoh Xil Basin	34.60	93.00	-3.972	-6.529	0.660	0.037	3.375	-1.514	Cyr et al. (2005)
Huaitoutala	37.30	96.70	-5.998	-4.418	-1.473	-3.620	3.104	0.409	Zhuang et al. (2011)
India Siwaliks	30.35	77.60	-1.862	0.006	0.103	-0.303	0.183	-1.851	Ghosh et al. (2004)
Luji Siwaliks	30.34	77.60	-1.862	0.006	0.103	-0.303	0.183	-1.851	Ghosh et al. (2005)

Janggalsay	38.15	86.62	-4.487	-2.406	1.026	-2.347	-0.952	0.192	Kent-Corson et al. (2009)
Jianchuan									
Basin	26.60	99.80	-1.356	-1.574	0.634	0.171	0.497	-1.083	Hoke et al. (2014)
Jingou	44.75	85.40	1.073	-0.031	1.270	1.435	-2.054	0.453	Charreau et al. (2012)
Kailas Basin	31.20	81.00	-6.705	-7.181	0.401	0.799	3.162	-3.886	DeCelles et al. (2011)
Kuitun	45.00	84.75	1.073	-0.031	1.270	1.435	-2.054	0.453	Charreau et al. (2012)
Lake Mahai	37.66	94.24	-0.964	-0.003	2.737	0.423	-4.188	0.066	Kent-Corson et al. (2009)
Lanping	26.50	99.40	-1.356	-1.574	0.634	0.171	0.497	-1.083	Hoke et al. (2014)
Lao Mangnai	36.94	91.96	-1.133	-3.998	0.447	0.356	2.233	-0.171	Kent-Corson et al. (2009)
Lenghu	37.84	93.36	-0.964	-0.003	2.737	0.423	-4.188	0.066	Kent-Corson et al. (2009)
Linxia Basin	35.69	103.10	0.443	-0.961	1.079	0.364	-0.410	0.371	Dettman et al. (2003)
Linzhou									
Basin	30.00	91.20	-6.756	-5.956	2.337	-0.057	0.886	-3.965	Ding et al. (2014)
Luhe	25.20	101.30	-0.242	0.009	0.317	0.411	-0.236	-0.742	Hoke et al. (2014)
Lulehe	37.50	95.08	-0.061	-0.987	1.724	1.950	-3.326	0.578	Kent-Corson et al. (2009)
Lulehe	37.50	95.08	-0.061	-0.987	1.724	1.950	-3.326	0.578	Kent-Corson et al. (2009)
Lunpola									
Basin	32.06	89.75	-6.763	-6.073	1.920	-0.652	1.561	-3.520	Rowley and Currie (2006)

Miran River	38.98	88.85	-4.786	-1.387	1.069	-2.683	-2.068	0.283	Kent-Corson et al. (2009)
Nepal									
Siwaliks	27.42	82.84	-1.370	0.006	-0.016	0.203	0.025	-1.588	Quade et al. (1995)
Nima Basin	31.75	87.50	-5.897	-7.724	-0.205	1.312	4.078	-3.359	DeCelles et al. (2011)
Oiyug Basin	29.70	89.50	-10.39	-7.842	2.634	-2.598	1.151	-3.735	Currie et al. (2005)
Oytug	38.98	75.51	-0.499	-0.716	1.320	0.719	-1.975	0.152	Bershaw et al. (2011)
Pakistan									
Siwaliks	33.39	73.11	0.645	0.008	0.380	0.407	0.379	-0.529	Quade et al. (1995)
Puska	37.12	78.60	-2.598	0.006	0.896	-0.472	-3.909	0.882	Kent-Corson et al. (2009)
Taatsin Gol	45.42	101.26	-0.731	-0.003	1.600	-0.364	-3.087	1.123	Caves et al. (2014)
Thakkhola	28.70	83.50	-4.018	-1.529	0.802	-0.310	-0.572	-2.409	Garziona et al. (2000)
Thakkhola-									
Tetang	28.66	83.50	-4.018	-1.529	0.802	-0.310	-0.572	-2.409	Garziona et al. (2000)
Xiao Qaidam	37.03	94.88	1.614	-1.376	1.772	3.117	-2.581	0.681	Kent-Corson et al. (2009)
Xifeng	35.70	107.60	0.245	0.00	0.522	0.173	-0.010	-0.440	Jiang et al. (2002)
Xorkol	39.01	91.92	-3.218	-0.871	1.871	-1.302	-2.970	0.054	Kent-Corson et al. (2009)
Xunhua Basin	35.90	102.50	0.443	-0.961	1.079	0.364	-0.420	0.371	Hough et al. (2010)
Yanyuan	27.50	101.50	-0.350	-1.152	0.657	0.539	0.373	-0.767	Hoke et al. (2014)

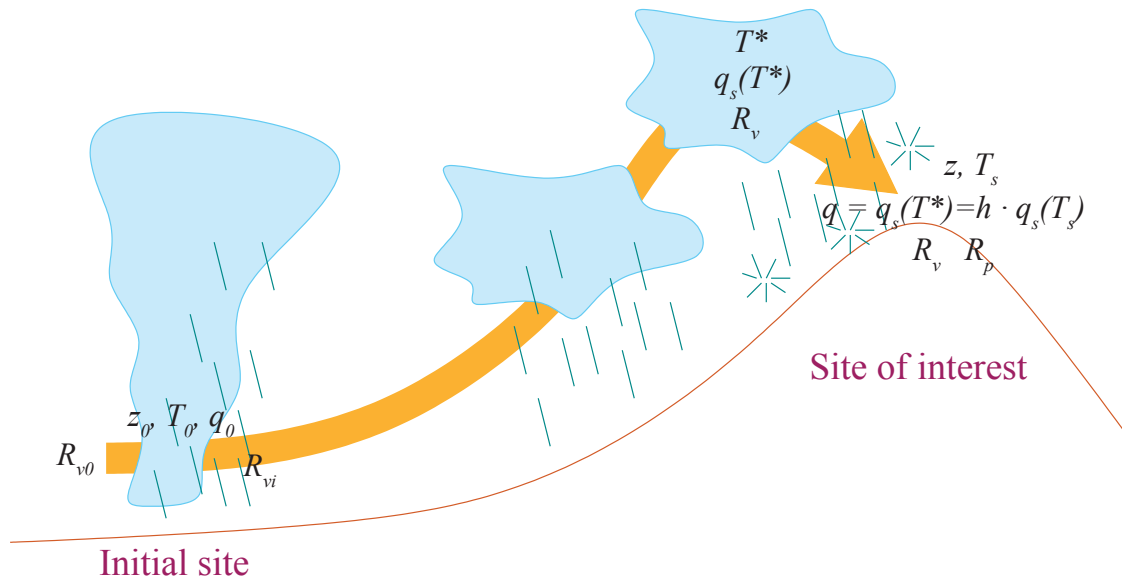
Zhada Basin	31.50	79.75	-3.983	-4.818	-0.046	0.831	2.708	-2.657	Saylor et al. (2009)
-------------	-------	-------	--------	--------	--------	-------	-------	--------	----------------------

1



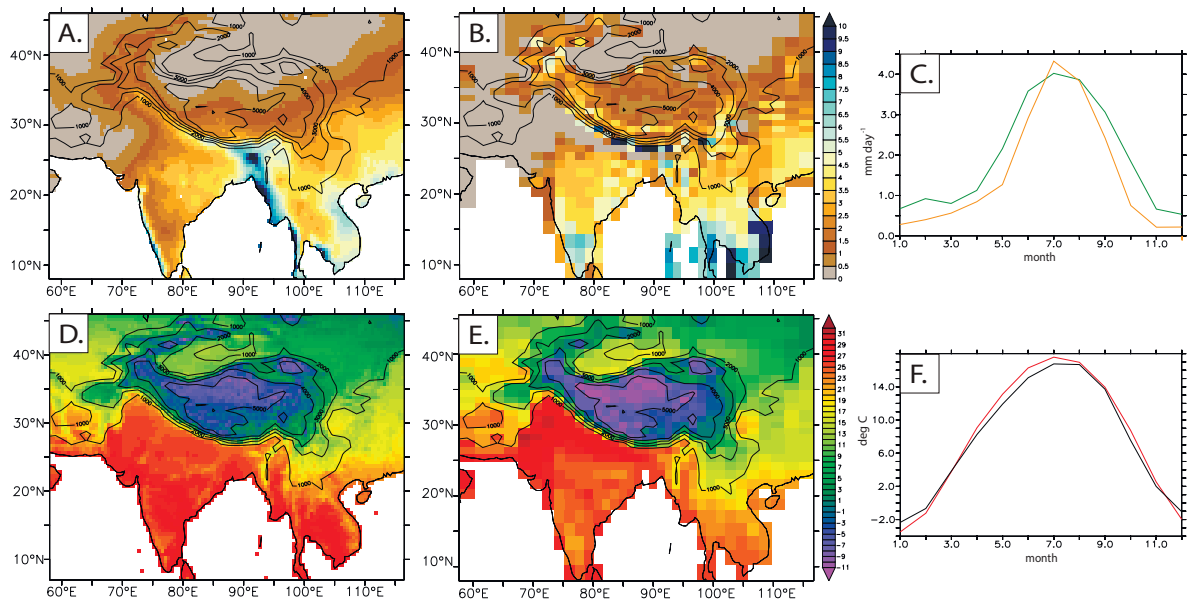
1
2
3
4
5
6
7
8
9
10

Figure 1. Models design (A) 100% of modern topography - MOD case; (B) Tibetan Plateau, Himalayas, Tian Shan, Pamir, Kunlun and Hindu Kush elevations reduced to 50% of modern elevation - INT case; (C) Tibetan Plateau, Himalayas, Tian Shan, Pamir, Kunlun and Hindu Kush elevations reduced to 250 m - LOW case. **Black rectangles show the division of the TP by regions: southern TP (between 25°N and 30°N), central TP (between 30°N and 35°N) and northern TP (between 35°N and 40°N).**



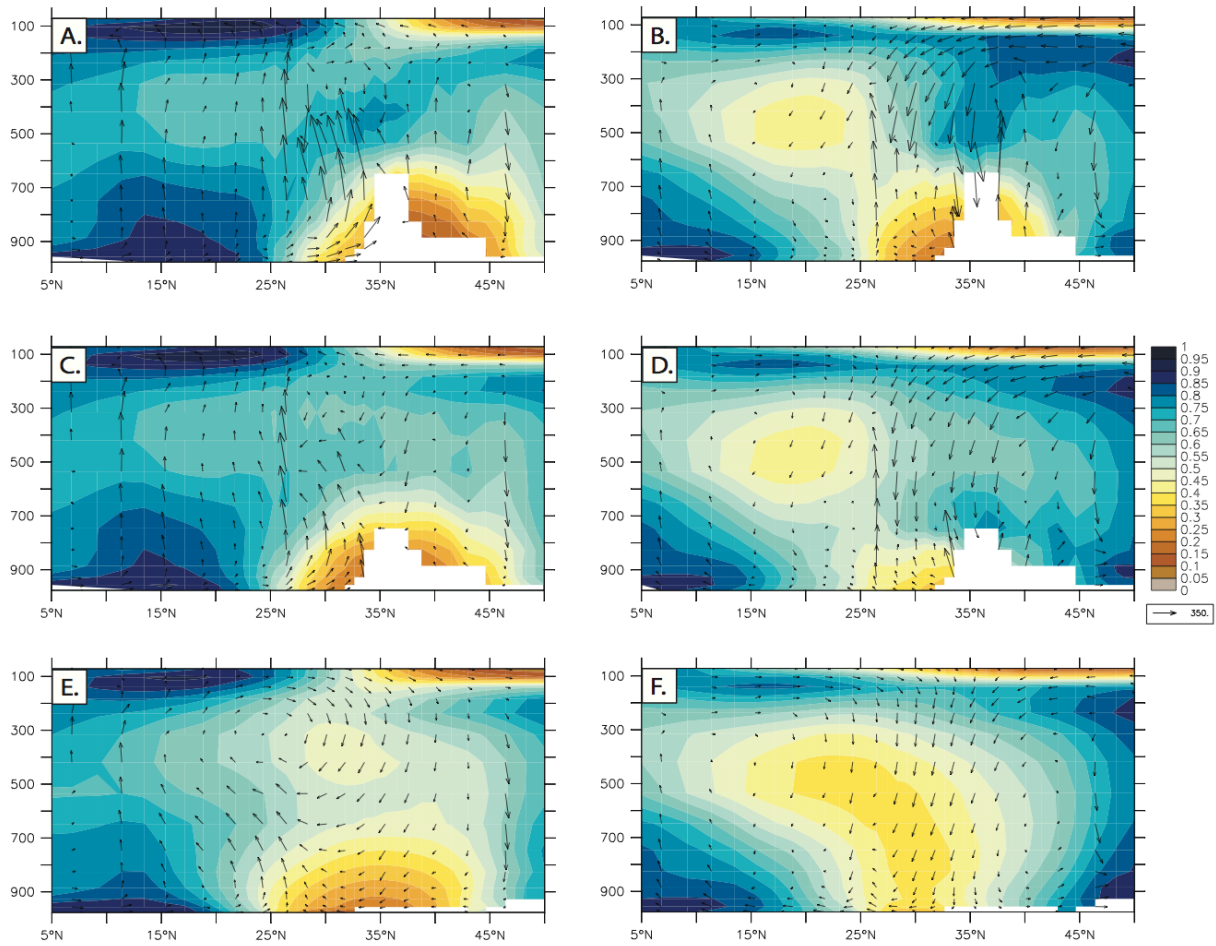
- 1
- 2
- 3
- 4
- 5
- 6
- 7
- 8
- 9

Figure 2. Idealized framework of an isolated air parcel transported from an initial site at low altitude to the site of interest. Most notations are illustrated.



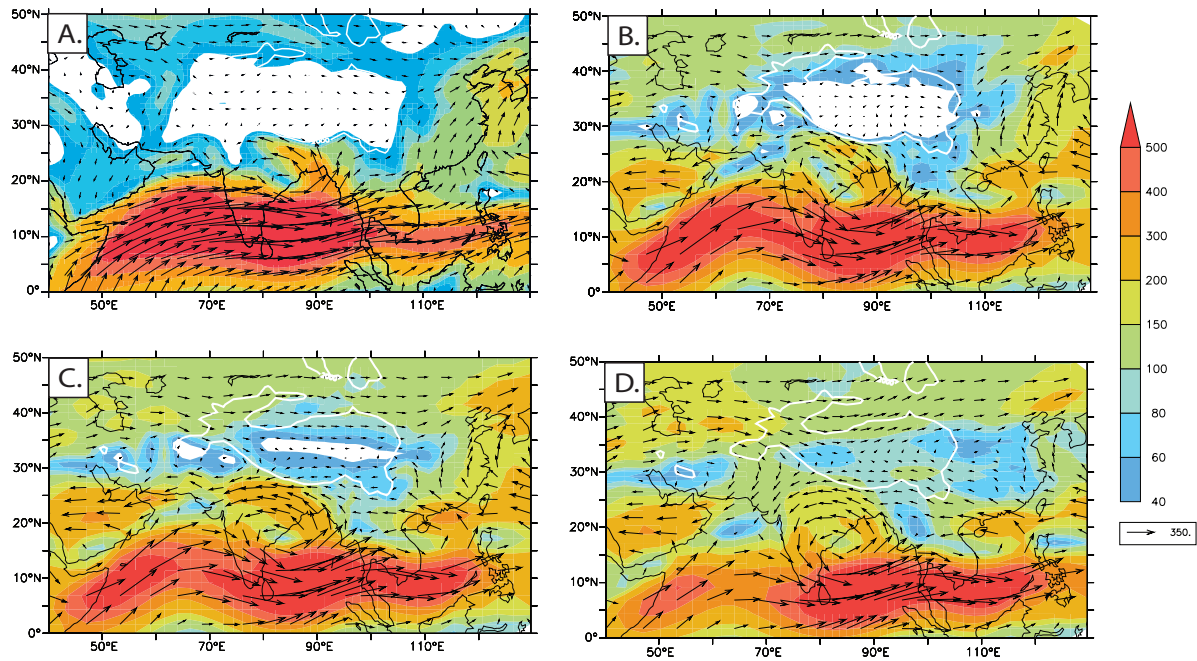
1
 2 **Figure 3. CRU dataset annual-mean rainfall (mm/day) (A) and annual-mean temperature (°C)**
 3 **(D) compared to simulated annual-mean rainfall for MOD experiment (B) and simulated**
 4 **annual-mean temperature for MOD experiment (E). The seasonal cycles of spatially averaged**
 5 **from 25°N to 40°N and from 75°E to 100°E for the MOD experiment precipitation (C) and**
 6 **temperature (F). Green and red lines of figures (C) and (F) corresponds for MOD experiment,**
 7 **orange and black to the CRU dataset respectively.**

8
 9
 10
 11
 12
 13
 14
 15



1
2
3
4
5
6
7
8
9
10
11
12
13

Figure 4. Cross-TP profiles (averaged between 70 and 90°E) showing the relative humidity and moisture transport for seasons (A, C, E) MJJAS and (B, D, F) ONDJFMA and for 3 simulation: (A, B) MOD, (C, D) INT, (E, F) LOW cases.



1

2

3 Figure 5. Directions and intensity of JJA vertically-integrated humidity transport for: (A)

4 averaged from ERA-40 re-analysis and for (B) MOD case, (C) INT case, (D) LOW case.

5

6

7

8

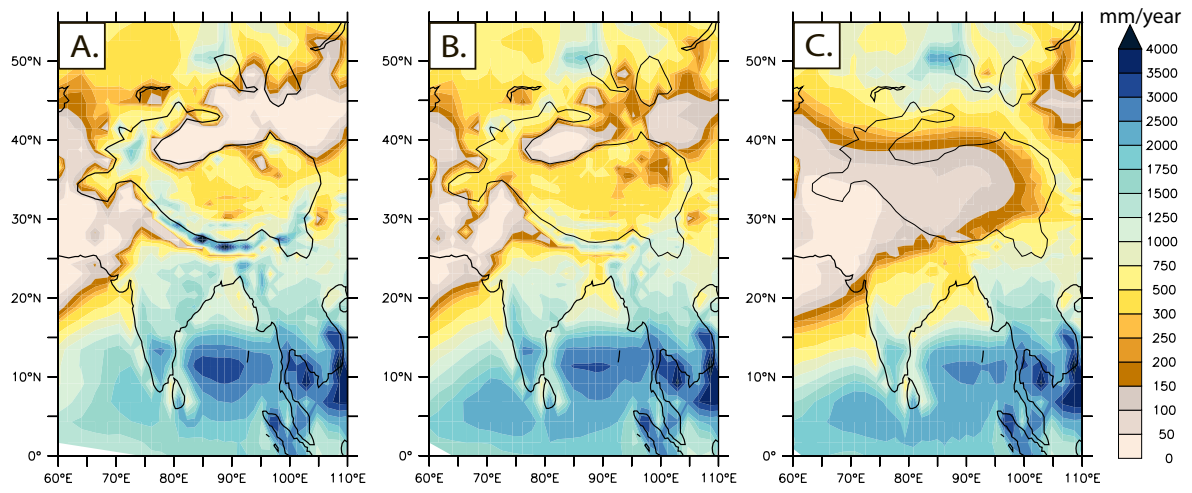
9

10

11

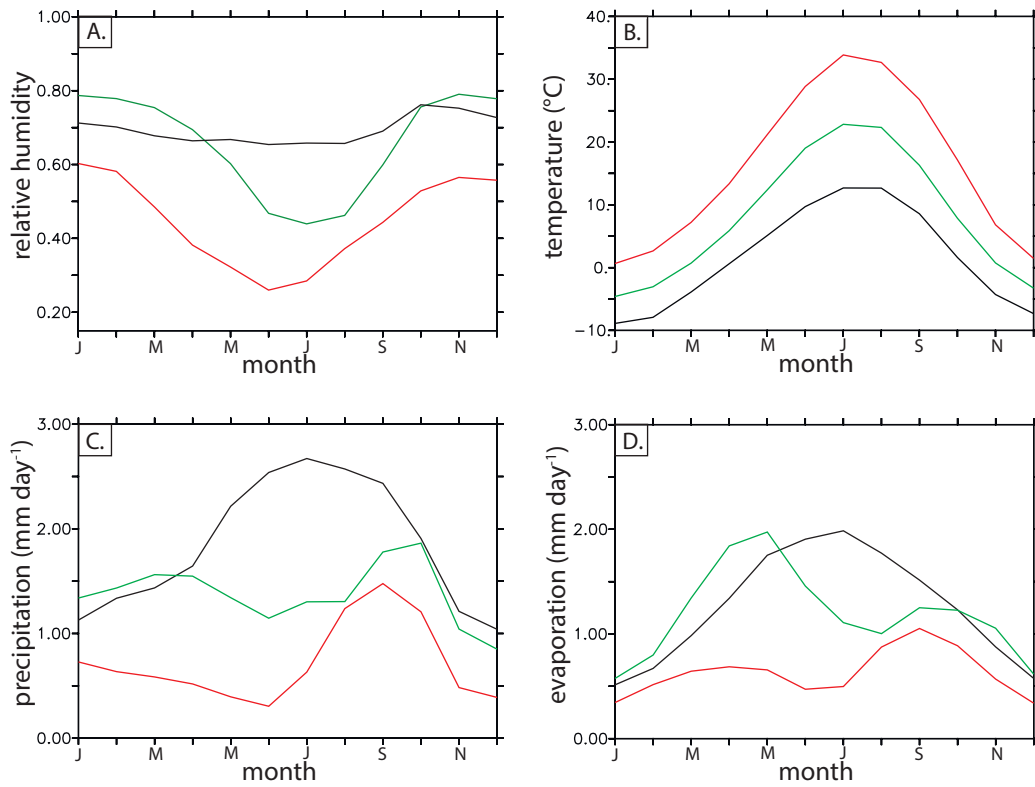
12

13



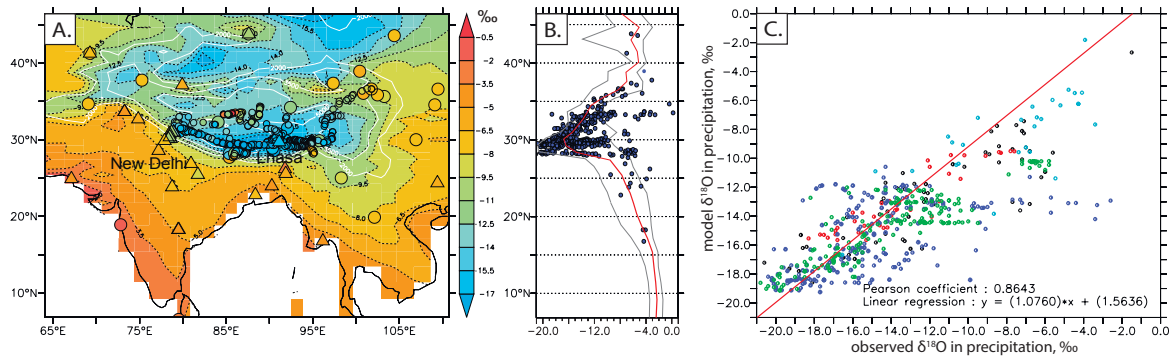
1
2
3
4
5
6
7
8
9
10
11
12
13
14
15
16
17
18
19

Figure 6. Annual mean precipitation amount (absolute values, mm/year) for: (A) MOD case, (B) INT case, (C) LOW case.



1
2
3
4
5
6
7
8
9
10
11
12
13
14
15

Figure 7. Intraannual variations in (A) low level relative humidity, (B) near-surface temperature, (C) precipitation amount and (D) evaporation amount. All variables are averaged for TP with the altitude over 1500 m. Black colour corresponds to MOD experiment, green - for INT experiment and red - for LOW experiment.



1

2 Figure 8. (A) Annual mean $\delta^{18}\text{O}$ in precipitation simulated by LMDZ-iso for MOD case.
 3 Triangles show $\delta^{18}\text{O}$ in precipitation from GNIP stations, big circles – $\delta^{18}\text{O}$ in precipitation
 4 from Caves et al. (2015) compilation (annual mean and JJA values respectively), small circles
 5 represent $\delta^{18}\text{O}$ in streams, lakes and springs compiled from Quade et al., 2011, Bershaw et al.,
 6 2012, Hren et al., 2009. (B) S-N profiles of model simulated $\delta^{18}\text{O}$ for the MOD case (. Blue
 7 points correspond to the same measured data as on panel A. The $\delta^{18}\text{O}$ profile is averaged
 8 between 75° E and 105° E. Grey lines show minimum and maximum values for the selected
 9 range of longitudes. (C) Observed vs. modelled $\delta^{18}\text{O}$ in precipitation. The colour corresponds
 10 of circles to the data set: red – Bershaw et al, 2012, blue – Quade et al, 2011, green – Hren et
 11 al, 2009, black – Caves et al, 2015, light blue show mean annual data from GNIP stations.
 12 Red line shows a linear regression.

13

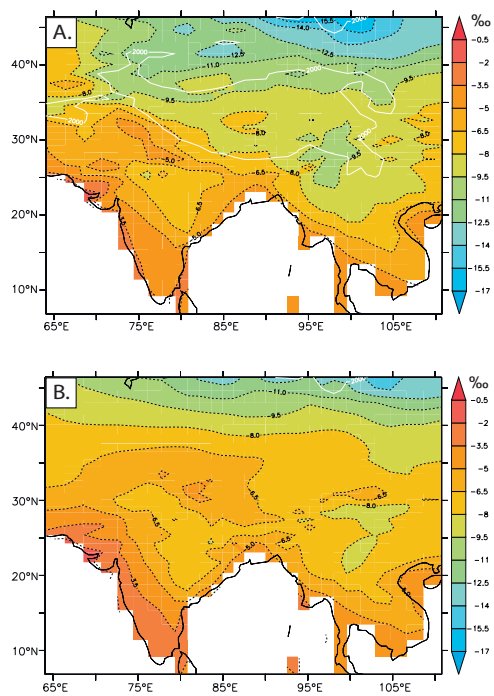
14

15

16

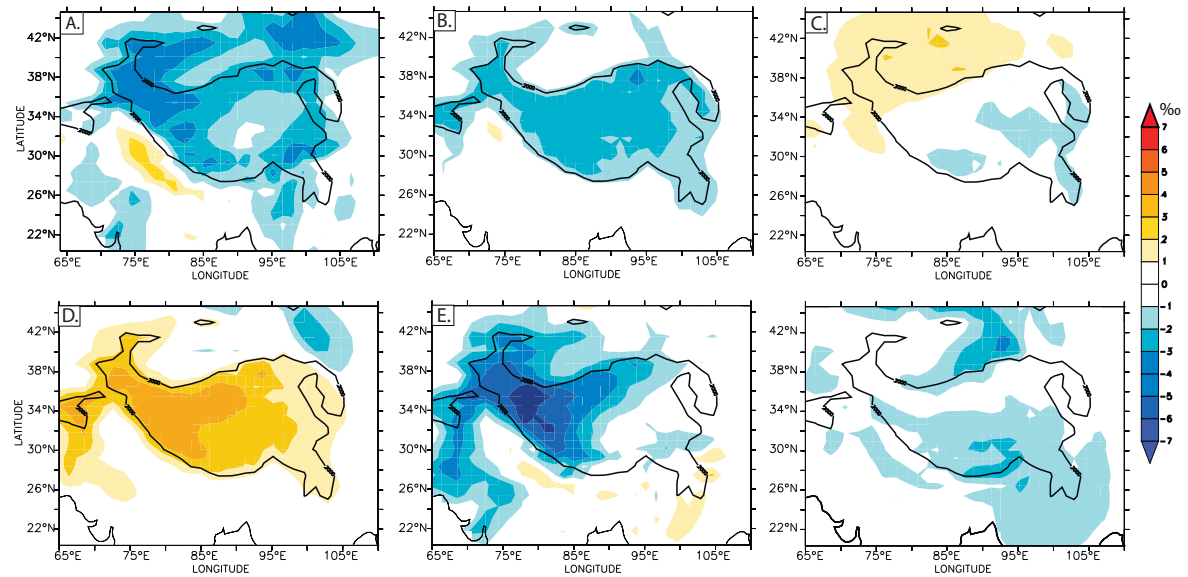
17

18



1
 2 **Figure 9. Annual mean $\delta^{18}\text{O}$ in precipitation simulated by LMDZ-iso for (A) INT case and**
 3 **(B) LOW case**

4
 5
 6
 7
 8
 9
 10
 11



1

2

3 Figure 10. (A) Total isotopic difference between INT and LOW experiments (ΔR_p) and spatial
 4 isotopic variations related to: (B) direct effect of topography changes, (C) effect of lapse rate
 5 change, associated with non-adiabatic effects, (D) effect of local relative humidity change, (E)
 6 effect of changes in post-condensational processes, (F) all other effect (see Table 1)

7

8

9

10

11

12

13

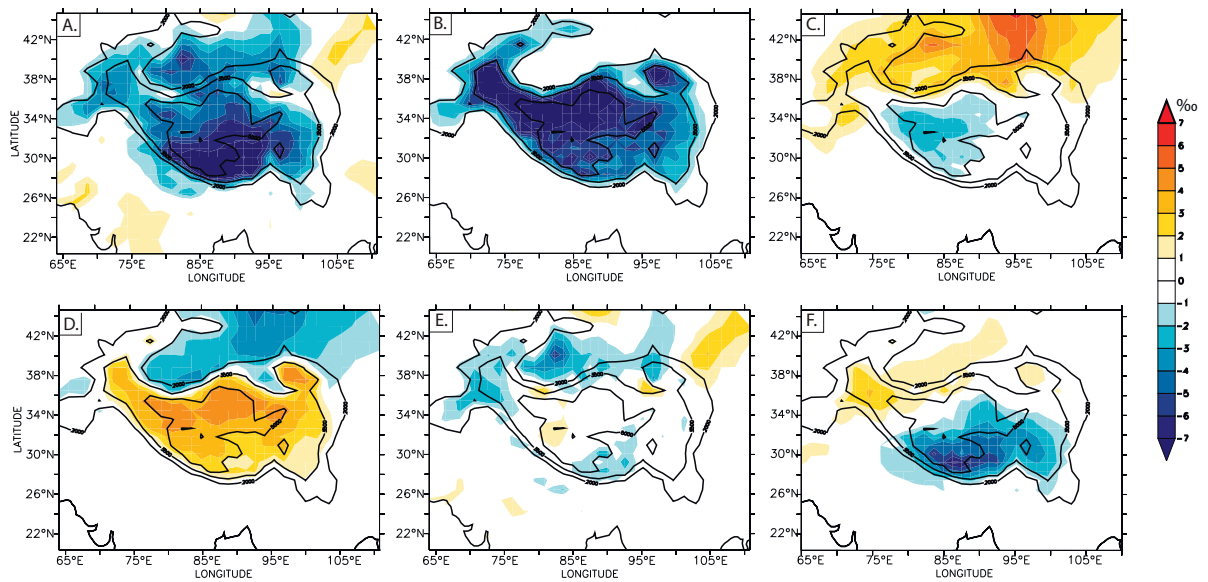
14

15

16

17

18



1

2

3 Figure 11. (A) Total isotopic difference between MOD and INT experiments (ΔR_p)
 4 and spatial isotopic variations related to: (B) direct effect of topography changes, (C) effect of
 5 lapse rate change, associated with non-adiabatic effects, (D) effect of local relative humidity
 6 change, (E) effect of changes in post-condensational processes, (F) all other effect (see Table
 7 1)

8

9

10

11

12

13

14

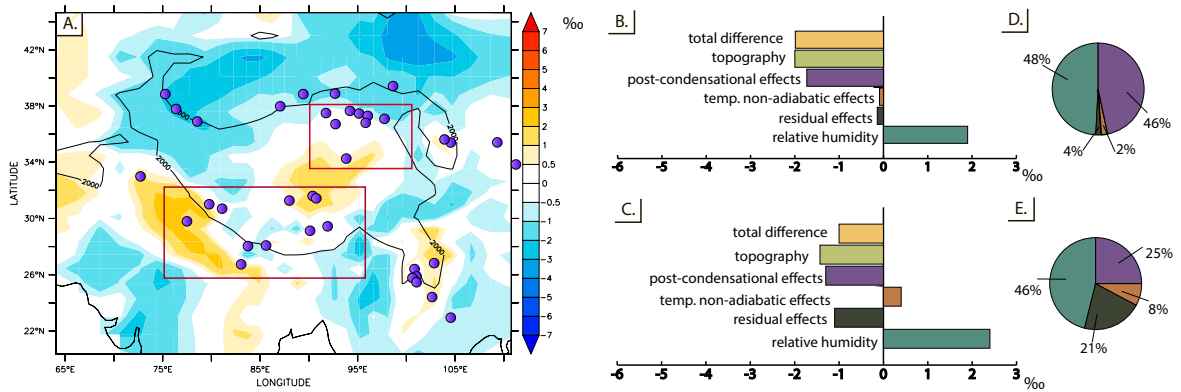
15

16

17

18

1



2

3

4 Figure 12. Difference in $\delta^{18}\text{O}_p$ between INT and LOW experiments that is not related to direct
 5 effect of topography changes. Violet points show Cenozoic paleoelevation studies locations
 6 (compiled from Caves et al., 2015). Red rectangles show regions for that averaged values
 7 decomposed terms are shown: B) Northern region, C) Southern region. Pie diagrams show
 8 portion of total isotopic difference related to processes other then topography: D) Northern
 9 region, E) Southern region

10

11

12

13

14

15

16

17

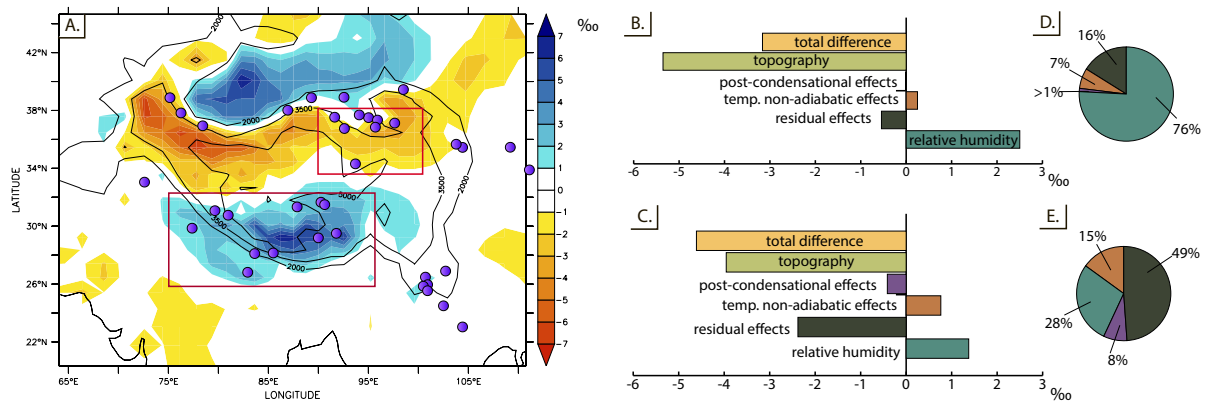
18

19

20

21

1



2

3 Figure 13. Difference in $\delta^{18}\text{O}_p$ between MOD and INT experiments that is not related to direct
4 effect of topography changes. Violet points show Cenozoic paleoelevation studies locations
5 (compiled from Caves et al., 2015). Red rectangles show regions for that averaged values
6 decomposed terms are shown: B) Northern region, C) Southern region. Pie diagrams show
7 portion of total isotopic difference related to processes other than topography: D) Northern
8 region, E) Southern region.

9

10

11

12

13

14

15

16

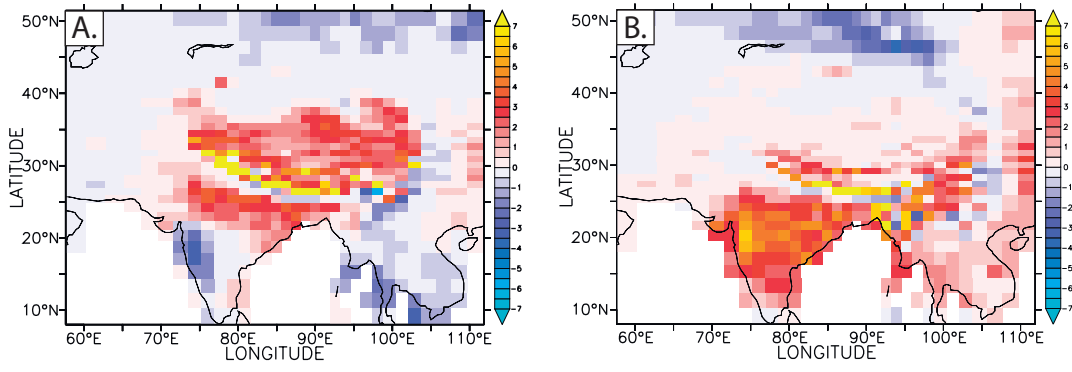
17

18

19

20

21



- 1
- 2
- 3
- 4
- 5
- 6
- 7

Figure 14. Precipitation change (mm/day) for A) MOD-INT B) INT-LOW cases